



On the importance of time delay and noise in thermoacoustic modeling



Francesco Gant^a, Giulio Ghirardo^a, Mirko R. Bothien^{b,*}

^a Ansaldo Energia Switzerland, Baden, Switzerland

^b ZHAW School of Engineering, Wintherthur, Switzerland

ARTICLE INFO

Article history:

Received 14 August 2020

Revised 26 February 2021

Accepted 1 March 2021

Available online 6 March 2021

Keywords:

Time delay

Thermoacoustics

Nonlinear

Dynamical system

Stochastic

ABSTRACT

Identification of thermoacoustic systems usually requires low-order modeling, often obtained by means of a Galerkin projection onto a single acoustic mode. The resulting dissipative self-excited oscillator equation describes the dynamic balance between acoustic energy sources (i.e. the flame) and sinks. Previous works studied the case of a nonlinear flame response and a driving background noise or a nonlinear delayed flame response in a deterministic setting. In the present work, we extend previous efforts considering a generic nonlinear delayed flame response with noise. In the case where both the delay and the noise are considered, we show that the widely-used cubic nonlinear saturation function is inadequate because it can lead to diverging solutions, due to the unboundedness of the respective describing function. We present an analytical treatment for a generic saturation function, which is benchmarked against an arctangent saturation function which does not exhibit this shortcoming. From a linear stability analysis, the delayed equation is found to present intrinsic thermoacoustic (ITA) eigenvalues, showing that a one-mode approximation can still retain information on both the acoustic and the ITA dynamics if a delayed flame model is adopted. Additionally, the model is found to present rich nonlinear dynamics (e.g. bistability) and to reproduce mode switching between two close frequencies, which is a feature often observed experimentally in thermoacoustic systems. We show that the derivation of quantitatively accurate equations for the slowly varying amplitude and phase is not trivial. To this regard, three sets of equations are introduced and a detailed discussion is dedicated to investigate their capability to model the original system dynamics. It is concluded that, for thermoacoustic applications, one of the presented sets more accurately models the delayed interaction between the acoustics and the flame response and should therefore be considered for system identification purposes. Additionally, a statistical characterization of the oscillation shows the need for more advanced modeling of amplitude and phase processes. We present novel equations based on perturbation methods and benchmark them with respect to classical results. The study explores a large nondimensional parameter space which encompasses a wide range of thermoacoustic systems.

© 2021 Elsevier Ltd. All rights reserved.

* Corresponding author.

E-mail address: both@zhaw.ch (M.R. Bothien).

1. Introduction

Lean-premixed gas turbines combustors are susceptible to thermoacoustic instabilities. In industrial applications, one often needs reliable models for experimentally observed thermoacoustic modes; these provide the starting point for implementing mitigation and suppression strategies, e.g. damper design [1]. A common methodology [2] is based on a Galerkin projection of the acoustic pressure field onto an acoustic mode of the combustor. As detailed in Ghirardo et al. [2], a single-degree-of-freedom second-order oscillator equation is obtained:

$$\ddot{\eta}(t) + \omega_0^2 \eta(t) = Q[\eta, \dot{\eta}] - \alpha \dot{\eta}(t) + \sigma \xi(t) \tag{1}$$

where $\dot{\eta}(t)$ is the acoustic pressure, $Q[\eta, \dot{\eta}]$ models the flame response, $\sigma \xi$ the background combustion noise, and $-\alpha \dot{\eta}$ is a damping term. A more detailed discussion of Eq. (1) is given in Section 2.

The challenge of studying, understanding and identifying the dynamical system in Eq. (1) [2] or its time derivative [3,4] has been extensively tackled in the last two decades. These works have been focused on the effect of the nonlinearity $Q[\eta, \dot{\eta}]$ and of the noise term $\sigma \xi$ on the oscillations. In the present work, we aim at extending the aforementioned contributions by introducing a *delayed* flame response function $Q[\dot{\eta}(t - \tau)]$, retaining at the same time a nonlinear flame response model *and* a noise-driven forcing of the system. The delay τ is well known to control the thermoacoustic stability of the system since the origin of this discipline [5], nevertheless only in very few works this has been introduced in the single Galerkin mode expansion Eq. (1), e.g. [6]. For example Crawford et al. [7,8] introduce a time-delayed flame transfer function, hence but limiting their investigations to a linear response, and therefore failing in predicting the existence of a limit-cycle solution. Ghirardo et al. [9] instead consider a delayed nonlinear model as in Eq. (3), but do so in a completely deterministic framework. This renders [9] not suited to a system identification and experimental perspective, because oscillation amplitude and phase are deterministic quantities and not distributions as is the case for experimental data. Very recently Bonciolini et al. [10] study a delayed flame model and investigate the effect of a Gaussian distributed time delay on the oscillations.

For the theoretical and numerical scope of this work, an analytical expression for the flame response function $Q[\eta, \dot{\eta}]$ is required. Usually, a cubic approximation [3,11,12] is introduced, with a parameter β to model the flame strength and a parameter k_c to describe the flame nonlinear saturation:

$$Q[\eta, \dot{\eta}] = \beta \dot{\eta} - k_c \dot{\eta}^3 \tag{2}$$

This is theoretically justified as Taylor expansion of the flame response, where the even powers can be neglected [4,11]. In the present work we consider a different model for the flame response:

$$Q[\dot{\eta}(t - \tau)] = \frac{\beta}{k} \text{atan}(k \dot{\eta}(t - \tau)) \tag{3}$$

The parameters β and k fulfill the same role as β and k_c in Eq. (2), modeling the linear and nonlinear flame response. The last term τ is the time delay between the acoustic pressure fluctuation at the flame location and the heat release fluctuation as response to the acoustic perturbation. The main difference between Eqs. (2) and (3) is that the nonlinearity in Eq. (3) is dynamic, whereas the nonlinearity in Eq. (2) is static. This means that in Eq. (3) the flame can respond both in phase and out of phase with respect to the pressure input $\dot{\eta}$ [9]. Additionally, in Eq. (3) the nonlinear function is modeled by an arctangent. By doing so, the physical requirement of the flame response to saturate to a finite value for large acoustic fluctuations, $|\dot{\eta}| \rightarrow +\infty$, is satisfied. This is important to guarantee the solutions to be bounded. Two time domain simulations of Eq. (1) are reported in Fig. 1. The results shown in the right plot are obtained by using a delayed arctangent model for the flame describing function (Eq. (3)), whereas in the left plot results for a delayed cubic model $Q[\dot{\eta}] = \beta \dot{\eta}(t - \tau) - k \dot{\eta}^3(t - \tau)$ are

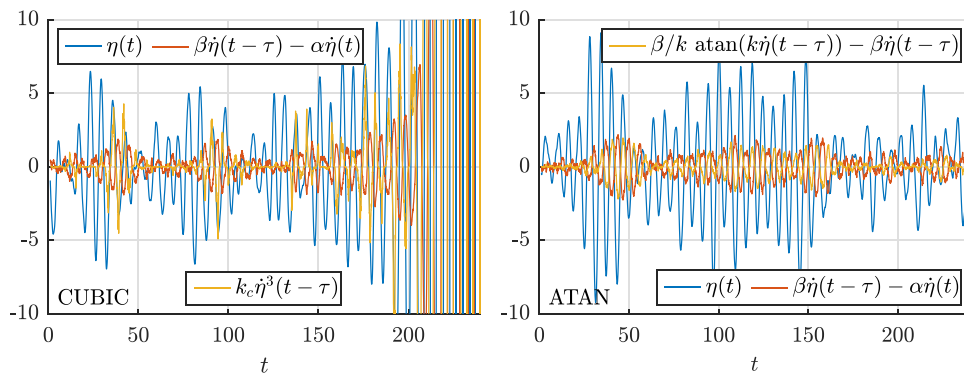


Fig. 1. Time domain simulation of the thermoacoustic oscillator Eq. (1) with a delayed flame model $Q = Q[\dot{\eta}(t - \tau)]$. Left: cubic model for the flame describing function (Eq. (2) delayed). Right: arctangent model for the flame describing function (Eq. (3)). The noise triggers an unstable behavior when the nonphysical cubic describing function is used.

shown. The parameters α , β , ω_0 , τ and σ are the same in both simulations. The nonlinear saturation constants k and k_c have been chosen differently for the two cases so that the limit-cycle amplitude of oscillation \hat{A} is the same. In the left plot of Fig. 1, it can be observed that the solution increases to infinity. Even if the limit cycle solution is linearly stable, the oscillation can become unstable. This phenomenon can be observed also by studying the corresponding deterministic system if the initial conditions are chosen accordingly. In a stochastic framework, this is not necessary: the noise causes the system to continuously explore new states and this can trigger an instability, as depicted in Fig. 1. The arctangent model, on the contrary, guarantees always bounded oscillations. This is related to the mathematical property of an arctangent describing function to saturate to a finite value and not to grow indefinitely as a cubic model. The widely-spread cubic model must therefore be used with caution and one needs always to verify that the studied system is non-delayed. In the present work, an arctangent model, Eq. (3), is used.

1.1. Aim and organization of this work

The present work aims at studying the single mode Galerkin projection Eq. (1) including all following three aspects: a nonlinear flame transfer function Eq. (3), depending on a delayed pressure signal $\hat{\eta}(t - \tau)$ and stochastically forced by a white noise $\sigma\xi$. In particular, we are interested in how the original system's physics are retained and how this affects the system stability, limit cycle behavior as well as stationary statistics. This is a novel contribution extending deterministic models [9] to stochastic and linear [7] to nonlinear ones. The mathematical analysis of Eq. (1) will be carried out following typical steps for nonlinear dynamical systems. The discussion will be accompanied by linking the findings to physical phenomena and highlighting their practical implications. Differences to a non delayed flame model Eq. (2) will be explained.

The paper is organized as follows: in Section 2, Eq. (1) is briefly derived and commented, introducing important literature contributions. In Section 3, Eq. (1) is nondimensionalized and the parameter ranges are defined. In Section 4 we briefly consider the linearized version of Eq. (1) and show some interesting results of the appearance of intrinsic thermoacoustic modes (ITA modes). The nonlinear framework is recovered in Section 5 where the dynamics are projected onto the slowly varying amplitude A and phase φ of oscillation. Subsequently, a discussion (Section 6) and comparison with numerical data (Section 7) is made. An accurate analysis of the amplitude and phase statistics is carried out in Sections 8 and 9, respectively. Section 10 then explores the parameter space of the nonlinear flame saturation.

2. Model derivation

In this section, we briefly derive Eq. (1), the starting point of this work, and discuss in detail the physical meaning of its terms.

The governing equations for acoustic pressure and velocity in a three dimensional geometry with a volumetric heat release source term are [13]:

$$\frac{1}{c^2} \frac{\partial p}{\partial t} + \rho_0 \nabla \cdot \mathbf{u} = \frac{\gamma - 1}{c^2} q \quad (4a)$$

$$\rho_0 \frac{\partial \mathbf{u}}{\partial t} + \nabla p = 0 \quad (4b)$$

where $\mathbf{u}(\mathbf{x}, t)$ and $p(\mathbf{x}, t)$ are the acoustic velocity and pressure fields, $\gamma(\mathbf{x})$ is the heat capacity ratio, $\rho_0(\mathbf{x})$ the mean density, $c(\mathbf{x})$ the speed of sound and $q(\mathbf{x}, t)$ the fluctuating heat release rate. The spatial and temporal coordinates are given by \mathbf{x} and t respectively. The combination of Eqs. (4a) and (4b) results into the inhomogeneous wave equation:

$$\frac{1}{c^2} \frac{\partial^2 p}{\partial t^2} - \gamma \nabla \cdot \left(\frac{\nabla p}{\rho_0} \right) = \frac{\gamma - 1}{c^2} \frac{\partial q}{\partial t} \quad (5)$$

A common strategy to solve Eq. (4) is through a Galerkin expansion [14,15], which requires a series expansion of the pressure and velocity fields:

$$p(\mathbf{x}, t) = \sum_{i=0}^{\infty} \hat{\eta}_i(t) \Psi_i(\mathbf{x}) \quad (6a)$$

$$\mathbf{u}(\mathbf{x}, t) = - \sum_{i=0}^{\infty} \eta_i(t) \frac{\nabla \Psi_i(\mathbf{x})}{\rho_0} \quad (6b)$$

Here, the functions $\eta_i(t)$ are unknown time dependent coordinates, whereas $\Psi_i(\mathbf{x})$ are admissible space functions. The set $\{\Psi_i(\mathbf{x})\}_{i=0}^{\infty}$ can be arbitrarily chosen as long as it is a complete basis and satisfies the spatial boundary conditions of the problem. Since the perturbation term q is usually small in thermoacoustic applications, a common approach consists in selecting the functions $\Psi_i(\mathbf{x})$ as the eigenmodes of the homogeneous problem $q = 0$ and studying how the introduction of the unsteady heat release rate q affects the natural oscillations of the system. As detailed in Ghirardo et al. [2], substituting

Eq. (6) into Eq. (4) and making use of the orthogonality of the functions $\Psi_i(\mathbf{x})$, a single-degree-of-freedom second order oscillator is obtained:

$$\ddot{\eta}(t) + \omega_0^2 \eta(t) = Q[\eta, \dot{\eta}] - \alpha \dot{\eta}(t) + \sigma \xi(t) \quad (1)$$

Eq. (1) is a second order stochastic nonlinear differential equation describing the temporal evolution of $\eta(t)$, obtained by the projection of the acoustic field onto the selected function $\Psi_i(\mathbf{x})$. In the homogeneous case, i.e. in the absence of acoustic energy sources and sinks, oscillations occur at the natural frequency of the system ω_0 . The presence of a flame (source) introduces two forcing terms: $Q[\eta, \dot{\eta}]$ and $\sigma \xi$. The former is a deterministic nonlinear operator modeling the flame response to fluctuations in acoustic pressure $\dot{\eta}(t)$ and velocity $\eta(t)$ [3,16]. The latter describes the background noise, i.e. non-coherent heat release fluctuations caused by different physical mechanisms [17]. Typically [4,18,19], this is approximated by a white Gaussian noise $\sigma \xi$ with standard deviation σ . This broadband spectrum assumption is very convenient analytically and it has been recently justified [19] as accurate for the single mode of Eq. (1). The splitting of the heat release into a sum of a deterministic and a stochastic contribution is common in the literature [2,20,21]. Retaining the stochastic contribution is particularly important for practical purposes, since it is the term directly responsible for the distributions and the statistics observed in experimental data. The remaining term to discuss in Eq. (1) is the damping term $-\alpha \dot{\eta}$, which appears when projecting Eq. (5) as a boundary term caused by reflection/transmission of acoustic energy through the domain inlet and outlet [2,21]. Eq. (1) contains all typical thermoacoustic ingredients (an acoustic field, a flame and some boundary conditions¹) in an elegant, one dimensional formulation, which is both based on a solid theoretical background [2,14,15] and on a vast amount of experimental validations [4,6,23–25]. Its simplicity, accuracy for predictions [26], and straightforward utilization in applied system identification [2,4] are the main reasons for the success of this formulation. In the following, we will consider thermoacoustic systems for which a single thermoacoustic mode is of interest, and no interaction occurs between the considered mode and other close by modes. We exclude therefore situations where naturally more modes interact together: azimuthal modes [12,27,28], transversal modes [29,30] and closely spaced modes [23].

2.1. Literature review

We briefly review some works dedicated to Eq. (1) and relate them to the present study.

An obvious question is how accurate Eq. (1) is in representing the actual dynamics. The thermoacoustic community has naturally tried to answer this question relaxing one after another the approximations used to obtain Eq. (1). Bonciolini et al. [19] consider a colored-noise version of Eq. (1) and investigate the effects of the color of the noise on the identification procedure. It is concluded that the effect is marginal as long as a correct filtering window is applied on the timeseries, an equivalent white noise intensity is introduced, and the background noise correlation time is small compared to the acoustic period. The effects of pressure and velocity-coupled noises are scrutinized by Li [31] et al.. Waugh and Juniper [25] introduce a more complex nonlinear function Eq. (2) and discuss how the noise intensity can introduce stochastic switches of the system between two different basins of attractions: a stable zero solution and a limit-cycle. Dowling and Stow [32] investigate instead the introduction of a time delay in Eq. (2): the flame has a delayed response to acoustic pressure and velocity fluctuations. Depending on the relative phase between heat release and pressure, the flame can have a stabilizing (negative growth rate) or destabilizing (positive growth rate) effect on the fundamental acoustic mode. The model as in Dowling and Stow [32] is extremely simple, but captures well the presence of instability bands and the shift of the oscillation frequency from the fundamental one. The effect of the combustion noise is not taken into account and the flame response is kept linear. Ghirardo et al. [9] extend Dowling's and Stow's work [32] to a nonlinear flame response, drawing nonlinear stability maps for a spectrum of parameters that comprises typical ranges of damping and growth rates. The effect of the flame phase and of its slope on the thermoacoustic system stability and oscillation frequency is analyzed. The present work builds on the results of Dowling and Stow [32] and Ghirardo et al. [9] in terms of delay and its effects on the linear and nonlinear dynamics, and on Bonciolini et al. [19] to correctly model the stochastic forcing.

Different identification methodologies have been proposed to estimate the parameters in Eqs. (1) and (2) from experimental time series. Noiray and Schuermans [4] show that the power spectral density of the acoustic pressure (in the linear regime) and the stationary solution of the Fokker–Planck equation for the slowly varying amplitude and phase (in the nonlinear regime) can correctly capture experimental results. The methodology validation is carried out by means of an electro-acoustic oscillator and subsequent application on engine data show the method's capability to capture the system dynamics. Successive applications have been performed both on full-scale gas turbine data [33] and with experiments in a lab-scale combustion chamber [34]. The growth rate extraction capability has been verified with numerical simulations [35]. Identification of growth and damping rates from lab-scale experiments have been carried out also by other research groups [26,36]. Different identification methodologies have been proposed to overcome limits and improve the accuracy of predictions as presented by [4]. Boujo and Noiray [37] discuss an improvement of the Kramer–Moyal coefficients estimation by making use of the adjoint Fokker–Planck equation. This allows to reduce inaccuracies introduced by *finite-time effects* (i.e. the fact that timeseries are often sampled at a fixed finite sampling frequency) and finally improves a methodology already discussed in Noiray and Schuermans [4]. Ghirardo et al. [2] tackle the limitation of an analytical closed-form expression for

¹ Eq. (1) is usually derived assuming fully reflective boundary conditions, but also other boundary conditions can be treated with this formulation [2,14,15,22].

the heat release term Eq. (2). The cubic model in Eq. (2) guarantees a correct reproduction of the nonlinear flame response only in the vicinity of the Hopf bifurcation characterizing the transition from stable to unstable linear regime, but is quite limited otherwise. The gray box model as in Ghirardo et al. [2] elegantly overcomes these limitations and is proved to be of great use for layout of dampers. Very recently, Lee et al. [24] propose an experimental input-output system identification based on exciting the thermoacoustic system with different levels of background noise and fitting the resulting statistics onto the analytical model as in Noiray and Schuermans [4]. The results show good prediction capabilities even if the data is just acquired at conditions before reaching the Hopf bifurcation.

In the present work (Sections 8 and 9), the equations in which two widely-spread system identification methodologies [2,4,24,26,31] are based will be compared with numerical simulations of Eq. (1) by parametrically studying the influence of the delay τ .

3. Nondimensionalization and studied parameter range of the underlying equations

The starting point of this work is Eq. (1) with the ansatz of Eq. (3) for the flame response to acoustic perturbations:

$$\ddot{\eta}(t) + \omega_0^2 \eta(t) = \frac{\beta}{k} \text{atan}(k\dot{\eta}(t - \tau)) - \alpha \dot{\eta}(t) + \sigma \xi(t) \tag{7}$$

We perform now a change of variables, defining a new time $\tilde{t} = \omega_0 t$ and a new dependent variable $\tilde{\eta} = \omega_0 k \eta$. Eq. (7) becomes:

$$\tilde{\eta}''(\tilde{t}) + \tilde{\eta}(\tilde{t}) = \frac{\beta}{\omega_0} \text{atan}(\tilde{\eta}'(\tilde{t} - \tau \omega_0)) - \frac{\alpha}{\omega_0} \tilde{\eta}'(\tilde{t}) + \frac{k\sigma}{\sqrt{\omega_0}} \xi(\tilde{t}) \tag{8}$$

where the prime has been used to designate the derivative with respect to the new time \tilde{t} . The system dynamics depend on four parameters: the normalized flame gain β/ω_0 , the normalized damping α/ω_0 , the normalized delay $\tau\omega_0$ and the normalized noise intensity $k\sigma/\sqrt{\omega_0}$. The first three parameters are the same as those introduced by Ghirardo et al. [9]; the normalized flame gain β/ω_0 and the normalized delay $\tau\omega_0$ can be also easily related to the *flame potency* and the *non-dimensional flame lag* as defined by Silva and Polifke [38]. The correct choice of these values is crucial to guarantee the applicability to real thermoacoustic systems. Fortunately, a rich literature review exists [9] of typical experimental values. We decide to closely follow the study of Ghirardo and co-workers [9] and choose similar values to those considered in their section 2.4; this features the additional benefit that a straightforward comparison can be drawn with their results. In particular, we fix the level of acoustic damping to $\alpha/\omega_0 = 0.1$ and the flame strength to $\beta/\omega_0 = 0.25$. This leads to a linear growth rate ν/ω_0 in absence of a delay $\tau\omega_0 = 0$ of $\nu/\omega_0 = (\beta - \alpha)/(2\omega_0) = 0.075$, which can be considered a typical value for a thermoacoustic system from Table 1 of [9]. Since the main focus of the present study lies in the effect of the time delay $\tau\omega_0$ on the dynamics, we decide to consider a parametric variation of this quantity alone, keeping the others constant. In particular, following again [9], we consider a range $\tau\omega_0 = [0, 10\pi]$ for the delay. This means, for example, that a thermoacoustic mode at $f = 100$ Hz with a dimensional delay of $\tau = 5$ ms exhibits a nondimensional $\tau\omega_0$ of π .

An estimation of the nondimensional noise intensity level, $k\sigma/\sqrt{\omega_0}$, is very difficult to derive because it requires the knowledge of the background noise σ and of the flame nonlinear saturation constant k . Both parameters are difficult to identify and often not considered in the literature. Indeed, many experimental studies focus purely on the estimation of the thermoacoustic frequency of oscillation and on the growth rate $\nu = (\beta - \alpha)/2$. Even those which explicitly take into account σ and k in the analytical modeling [4,26], often do not present their estimated values. An exception to this are the works of Bonciolini et al. [19,21]. To overcome this difficulty, we proceed with an indirect method based on the statistics of the oscillation amplitude A . For this purpose, the envelope of the quasi-sinusoidal acoustic pressure oscillation η is considered (see Section 5 for a formal introduction). Different works [3,4] present experimental distributions of the system amplitude A , which is, for linearly unstable systems, usually bell-shaped around a mean value \bar{A} , see for example Fig. 7 of [4] or Fig. 8 of [3]. Typical values of the ratio between the amplitude swing ΔA and the mean value \bar{A} are estimated to be usually in the range $\Delta A/\bar{A} \approx [0.1 - 0.8]$. This ratio is directly related to the noise intensity σ , for which larger σ directly reflect larger ΔA . The estimation of the typical values for $k\sigma/\sqrt{\omega_0}$ has been carried out imposing the resulting amplitude distribution of Eq. (27) to present similar $\Delta A/\bar{A}$ ratios. This analysis suggests $k\sigma/\sqrt{\omega_0} \in [0.05, 0.25]$. We consider $k\sigma/\sqrt{\omega_0} = 0.15$ and discuss the effect of a modification of this value and of the other parameters α/ω_0 and β/ω_0 in Section 10.

In the following, we will keep the equations dimensional but discuss uniquely the dependence on the four normalized parameters β/ω_0 , α/ω_0 , $\tau\omega_0$ and $k\sigma/\sqrt{\omega_0}$.

Table 1

Summary of the properties of the averaged equations describing the evolution of the slowly varying quantities A and φ . The three sets of equations correspond to the three averaging methods used (HALE, WH and LW).

Method	Resulting equation type	Variables	Amplitude eq. with respect to phase eq.	Phase eq. with respect to amplitude eq.	References
HALE (18)	SDE	A, φ	Decoupled	Coupled	[49–52]
WH (20)	SDDE	A, A_τ, φ	Decoupled	Coupled	[58]
LW (19)	SDDE	$A, A_\tau, \varphi, \varphi_\tau$	Coupled	Coupled	[54–57]

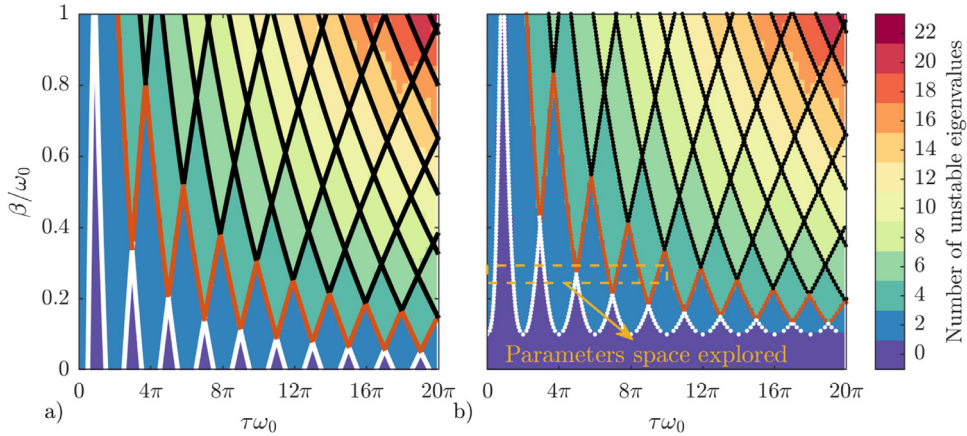


Fig. 2. Stability map of the linearized thermoacoustic oscillator Eq. (9) as function of the flame strength β/ω_0 and the normalized delay $\tau\omega_0$. The white, red and black lines are the boundaries of neutral stability obtained by solving Eq. (12) with $\nu = 0$. The colormap represents the number of unstable eigenvalues in each region, evaluated by Stepan's formula [39]. The white line marks the transition of the acoustic mode from stable to unstable. The red line marks the transition of the first ITA mode to instability. The dashed box highlighted in yellow in the bottom left corner of Fig. 2b represents the parameter space investigated in the discussion of the nonlinear regime. a) $\alpha/\omega_0 = 0$. b) $\alpha/\omega_0 = 0.1$. (For interpretation of the references to color in this figure legend, the reader is referred to the web version of this article.)

4. Linear stability and ITA modes

Before exploring the nonlinear regime we consider the linearized dynamics of the oscillator in Eq. (7) around a zero solution, in absence of combustion noise:

$$\ddot{\eta}(t) + \omega_0^2 \eta(t) = \beta \dot{\eta}(t - \tau) - \alpha \dot{\eta}(t) \quad (9)$$

Eq. (9) has been extensively studied in Ghirardo et al. [9]. We do not reproduce the full analysis presented in there but only briefly summarize the main results and focus on some new interesting aspects. The stability analysis is carried out substituting a complex exponential dependence for $\eta(t)$:

$$\eta(t) = e^{\lambda t} = e^{(\nu + i\omega)t} \quad (10)$$

where ν is the growth rate of the oscillation, and quantifies if the oscillation is growing ($\nu > 0$) or decaying ($\nu < 0$) in time, and ω is the associated frequency of oscillation. Next, Eq. (10) is substituted into Eq. (9):

$$\lambda^2 + \omega_0^2 = \beta \lambda e^{-\lambda \tau} - \alpha \lambda \quad (11)$$

The roots of the resulting system of nonlinear transcendental equations Eq. (11) are searched for:

$$R(\lambda) = \nu^2 - \omega^2 + \omega_0^2 - \beta(\nu \cos(\omega\tau) + \omega \sin(\omega\tau))e^{-\nu\tau} + \alpha\nu = 0 \quad (12a)$$

$$S(\lambda) = 2\nu\omega - \beta(-\nu \sin(\omega\tau) + \omega \cos(\omega\tau))e^{-\nu\tau} + \alpha\omega = 0 \quad (12b)$$

Each set (ν, ω) solving Eq. (12) is an eigenvalue of Eq. (9) and represents a potential oscillatory solution of Eq. (9). The number of eigenvalues of Eq. (12) is, in general, infinite; it is therefore not possible to track the evolution of all of them. A method by Stepan [39] allows to exactly compute how many eigenvalues are unstable for each given set of parameters $[\alpha/\omega_0, \beta/\omega_0, \tau\omega_0]$. We plot, for twice the range of $\tau\omega_0$ discussed in Section 3, for $\beta/\omega_0 \in [0, 1]^2$ and for two values of the acoustic damping ($\alpha/\omega_0 = 0$ and $\alpha/\omega_0 = 0.1$) the number of unstable eigenvalues in Fig. 2. The black, red and white lines represent the margin of neutral stability, i.e. the solution to Eq. (12) for $\nu = 0$. Every time a margin of neutral stability is crossed, one or more eigenvalues of Eq. (9) cross the imaginary axis, passing from stable to unstable or vice-versa. The purple regions represent stable domains, where all eigenvalues lie in the left part of the complex plane. Physically, the thermoacoustic system is stable and the acoustic oscillations are damped. For all other colored domains, the dynamic system is unstable: the acoustic pressure oscillations grow from 0 up to the condition where nonlinear phenomena saturate the growth and result in a limit-cycle (Section 6). The results as presented in Fig. 2 agree with Fig. 3 of Ghirardo et al. [9], showing how large flame gains β/ω_0 and flame phase slopes $\tau\omega_0$ render the thermoacoustic system more prone to instability.

We now track more precisely the eigenvalues' paths in the complex plane (Fig. 3). For this, we fix α/ω_0 and $\tau\omega_0 = 15$ and gradually increase the flame strength β/ω_0 from 0 to 1, tracking all eigenvalues in the domain $[\nu/\omega_0 \times \omega/\omega_0] = [-0.9, 0.1] \times$

² Realistic values are $\beta/\omega_0 \in [0, 0.3]$ according to Ghirardo et al. [9].

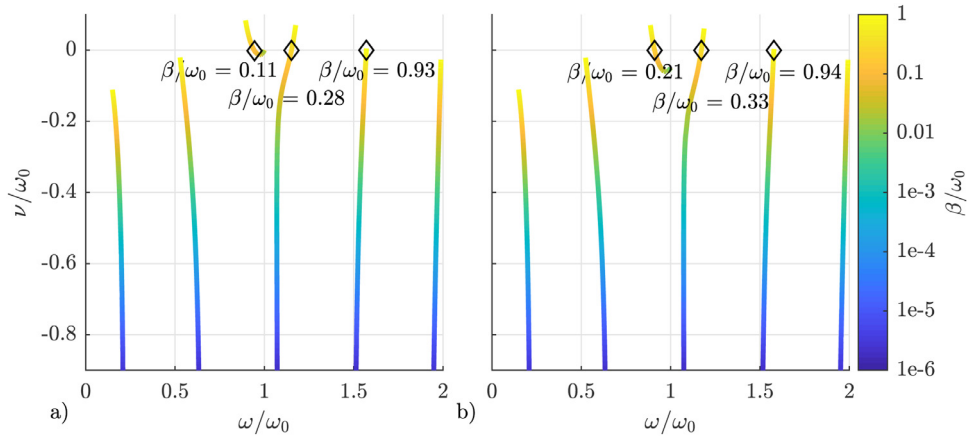


Fig. 3. Eigenvalues tracking for the linearized thermoacoustic oscillator Eq. (9) as the flame strength β/ω_0 is increased from 0 to 1. For $\beta/\omega_0 = 0$, the system oscillates at the acoustic mode $\omega/\omega_0 = 1$. As the flame strength β/ω_0 is increased, infinite ITA modes grows from $\nu/\omega_0 \rightarrow -\infty$ and affect the acoustic mode dynamics. In diamonds the crossing positions through the imaginary axis, with reported the corresponding β/ω_0 . Other parameters: $\tau\omega_0 = 15$, (a) $\alpha/\omega_0 = 0$, (b) $\alpha/\omega_0 = 0.1$.

[0, 2]. For $\beta/\omega_0 = 0$, Eq. (12) has the solution $[\nu/\omega_0, \omega/\omega_0] = [0, 1]$. In the absence of a flame, the system is neutrally stable and oscillating at the acoustic frequency ω_0 . When perturbing β/ω_0 from 0, an infinite number of other eigenvalues arise. They feature large, negative growth rates and are oscillating at frequencies $\omega = (2k + 1)\pi/\tau$ for $k = 0, 1, 2, 3, \dots$. As $\beta/\omega_0 \rightarrow 0$, the growth rate ν of these eigenvalues will approach $-\infty$, whereas as β/ω_0 increases their growth rate ν will approach 0. The presence of these solutions of the characteristic equation Eq. (12) has already been reported in the literature [32] and, according to the definition presented in Mukherjee and Shrira [40], Orchini et al. [41], these eigenvalues correspond to intrinsic thermoacoustic (ITA) modes. Differently said, it is here shown that Eq. (7) retains the projection of both acoustic modes and ITA modes onto the space function $\Psi_i(\mathbf{x})$. We remark that a projection in which a phase difference between the flame response and the acoustics is not allowed (i.e. $\tau = 0$), is not capable to retain the ITA dynamics of the original system.

For small values of the flame strength β/ω_0 , the ITA eigenvalues are present but are not visible in the system dynamics because they are strongly damped ($\nu \rightarrow -\infty$) and the acoustic eigenvalue is dominant. As β/ω_0 is increased, as observed in Fig. 3, the ITA eigenvalues approach the boundary of neutral stability and interact with the acoustic eigenvalue. The frequency of oscillation of the acoustic eigenvalue changes from ω_0 , the natural acoustic frequency of the mode, to ω , the thermoacoustic frequency of oscillation. For a critical value of β/ω_0 , depending on the slope of the flame phase $\tau\omega_0$, one of the eigenvalues of the dynamical system transits above the imaginary axis and the system becomes unstable. For the two cases considered in Fig. 3, both in presence and in absence of acoustic damping α/ω_0 , the first eigenvalue to become unstable is the acoustic one. This is represented in Fig. 2 by the white line marking the transition of the acoustic eigenvalue to instability. Increasing further β/ω_0 the ITA eigenvalues become, one by one, unstable. Nevertheless, for the ranges of parameters considered here, the acoustic eigenvalue always features the largest growth rate ν and is, therefore, the only eigenvalue observable. This is not in contradiction with literature works [40,42] where it has been shown that the thermoacoustic system can oscillate due to a pure ITA mode. In fact, Eq. (7) describes the projection of the acoustic field onto a particular function $\Psi_i(\mathbf{x})$, here chosen to be an acoustic eigenmode of the system without flame $q = 0$, and not the whole acoustic field. If one wishes to observe a pure ITA mode, this projection has to be done with respect to a different function $\Psi_i(\mathbf{x})$.

The presence of an acoustic damping term $\alpha/\omega_0 \neq 0$ modifies quantitatively but not qualitatively above observations as can be seen by comparison of Fig. 3(a) and (b).

5. The slowly varying equations

In order to study the nonlinear dynamics of Eq. (1), a more suitable approach than the direct analysis of η exists. Indeed, Eq. (1) is usually directly studied only if the flame response is kept linear [7,8], whereas it is common practice [4,9,43] to introduce a change of variables when the nonlinear behavior is of interest. This is explained in detail in Section 5.1. Given the presence of a delay $\tau\omega_0$ in Eq. (7), the common methods [44,45] utilized to derive the governing equations for the new variables are not applicable, and different new methods will be introduced (Sections 5.3–5.5).

5.1. Change of variables

As is common practice in thermoacoustics [4,9,43], the time domain equation describing the pressure evolution Eq. (1) can be mapped into a set of two coupled ordinary differential equations in two new variables: the slowly vary-

ing amplitude A and the slowly varying phase φ . The acoustic pressure $\dot{\eta}$ can be written as:

$$\dot{\eta}(t) = A(t) \cos(\omega t + \varphi(t)) \quad (13)$$

The amplitude A represents the envelope of the fast varying pressure signal in the time domain. It is a slowly varying quantity because it changes on a longer timescale than the oscillation period of the thermoacoustic mode of interest. The slowly varying phase φ is a measure of the shift of the oscillation frequency of the system from its thermoacoustic frequency ω . Eq. (13), in conjunction with the ansatz:

$$\eta(t) = A(t) \sin(\omega t + \varphi(t))/\omega \quad (14)$$

maps the original Eq. (1) into:

$$\dot{A} = f_A(A, A_\tau, \varphi, \varphi_\tau, t) + g_A(A, \varphi, t)\xi(t) \quad (15a)$$

$$\dot{\varphi} = f_\varphi(A, A_\tau, \varphi, \varphi_\tau, t) + g_\varphi(A, \varphi, t)\xi(t) \quad (15b)$$

where the subscript τ indicates a delayed variable, i.e. $A_\tau \triangleq A(t - \tau)$ and $\varphi_\tau \triangleq \varphi(t - \tau)$. The functions in Eq. (15) are defined as:

$$f_A(A, A_\tau, \varphi, \varphi_\tau, t) \triangleq + \left(\omega - \frac{\omega_0^2}{\omega} \right) A \sin \phi \cos \phi - \alpha A \cos^2 \phi + Q[\eta, \dot{\eta}, \eta_\tau, \dot{\eta}_\tau] \cos \phi \quad (16a)$$

$$f_\varphi(A, A_\tau, \varphi, \varphi_\tau, t) \triangleq - \left(\omega - \frac{\omega_0^2}{\omega} \right) \sin^2 \phi + \alpha \cos \phi \sin \phi - \frac{1}{A} Q[\eta, \dot{\eta}, \eta_\tau, \dot{\eta}_\tau] \sin \phi \quad (16b)$$

$$g_A(A, \varphi, t) \triangleq + \sigma \cos \phi \quad (16c)$$

$$g_\varphi(A, \varphi, t) \triangleq - \frac{1}{A} \sigma \sin \phi \quad (16d)$$

where $\phi \triangleq \omega t + \varphi$. Eq. (15) depend on two different timescales. In order to get insight into the slow dynamics of A and φ , one can integrate Eq. (15) over a thermoacoustic period $T = 2\pi/\omega$ and assume that the slowly varying quantities A, A_τ, φ and φ_τ stay constant over T . This procedure is known in the literature as *method of averaging* and it is standard in thermoacoustic system analysis [2,4,28], as well as in other disciplines [45,46]. One can find more details about the method of averaging in Sanders et al. [47] or in the original work of Krylov and Bogoliubov [48]. The presence of a stochastic forcing term in Eq. (1) requires the application of a modification of the method of averaging called *stochastic averaging*, as explained by Stratonovich [44] and reviewed by Roberts and Spanos [45].

In the present context though, the main difficulty lies in the presence of a delayed term. In the literature, there is no unique method of averaging for delayed differential equations. After introducing the concept of flame describing function, in Sections 5.3–5.5 we discuss and apply three possibilities.

5.2. Flame describing function

We introduce the concept of flame describing function $Q(A, \omega)$ [2], so that the results of Sections 5.3–5.5 can be expressed in a more general way, independent of the particular choice of the nonlinear saturation function $Q[\dot{\eta}]$, Eq. (3). The function $Q(A, \omega)$ is a complex-valued function that relates the output of the nonlinear system $Q[\dot{\eta}]$ to its input, when the input is a sinusoid $\dot{\eta} = A \cos(\omega t)$. In particular, for a given amplitude A and frequency ω of the input forcing, the function $Q(A, \omega)$ returns the amplitude $|Q(A, \omega)|$ and the phase $\angle Q(A, \omega)$ of the output at the frequency ω :

$$Q(A, \omega) \triangleq \frac{1}{A} \frac{1}{\pi/\omega} \int_0^{2\pi/\omega} Q[A \cos(\omega s)] e^{-i\omega s} ds = 2\beta \frac{\sqrt{k^2 A^2 + 1} - 1}{k^2 A^2} \quad (17)$$

where the last term is the analytic expression of the flame describing function when the nonlinear function is an arctangent, $Q[\dot{\eta}] = \beta/\text{katan}(k\dot{\eta})$.

5.3. The method of Hale (HALE method)

Tackling the problem of averaging delayed equations started to arise in the 1960s when different control system problems with delayed terms required averaging [49]. Different researchers worked at the same time on developing a theory of averaging delayed differential equations (DDE). One can find details in works of Medvedev [50], Halalay [51] and Foduck

[52]. A complete summary is provided in the work from Hale [49]. This approach is able to map a DDE to a set of ordinary differential equations (ODEs) for the slowly varying quantities, which are more straightforward to treat and discuss. Its application to Eq. (15) results in the following averaged equations:

$$\begin{aligned} \dot{A} &= \frac{1}{T} \int_0^T f_A(A, A_\tau = A, \varphi, \varphi_\tau = \varphi, s) ds + \frac{\sigma^2}{4A} + \frac{\sigma}{\sqrt{2}} \xi_1 \\ &= -\frac{1}{2} \alpha A + \frac{1}{2} A \cos(\omega\tau) \operatorname{Re}[\mathcal{Q}(A)] + \frac{1}{2} A \sin(\omega\tau) \operatorname{Im}[\mathcal{Q}(A)] + \frac{\sigma^2}{4A} + \frac{\sigma}{\sqrt{2}} \xi_1 \\ &= \underbrace{\frac{\beta}{k} \cos(\omega\tau) \frac{\sqrt{k^2 A^2 + 1} - 1}{kA}}_{F_H(A)} - \frac{1}{2} \alpha A + \frac{\sigma^2}{4A} + \frac{\sigma}{\sqrt{2}} \xi_1 \end{aligned} \quad (18a)$$

$$\begin{aligned} \dot{\varphi} &= \frac{1}{T} \int_0^T f_\varphi(A, A_\tau = A, \varphi, \varphi_\tau = \varphi, s) ds + \frac{\sigma}{A\sqrt{2}} \xi_2 \\ &= -\frac{1}{2} \left(\omega - \frac{\omega_0^2}{\omega} \right) + \frac{1}{2} \cos(\omega\tau) \operatorname{Im}[\mathcal{Q}(A)] - \frac{1}{2} \sin(\omega\tau) \operatorname{Re}[\mathcal{Q}(A)] + \frac{\sigma}{A\sqrt{2}} \xi_2 \\ &= \underbrace{-\frac{1}{2} \left(\omega - \frac{\omega_0^2}{\omega} \right) - \beta \sin(\omega\tau) \frac{\sqrt{k^2 A^2 + 1} - 1}{k^2 A^2}}_{G_H(A)} + \frac{\sigma}{A\sqrt{2}} \xi_2 \end{aligned} \quad (18b)$$

The terms ξ_1 and ξ_2 are independent Gaussian white noises with unitary standard deviation [44,53]. The averaging on the two functions f_A and f_φ is performed with the assumption that the delayed terms A_τ and φ_τ can be approximated by their non-delayed counterparts A and φ . In thermoacoustics this is usually accompanied by the hypothesis that the delay is relatively short [28] (order of magnitude of an acoustic period) and that therefore the delayed quantities A_τ and φ_τ can be interchanged with their non-delayed counterparts.

Note that the dot symbol in Eq. (18) represents now the derivative with respect to the slow time. This convention is valid for the rest of this manuscript.

5.4. The method of Lehman and Weibel (LW method)

The theory on averaging of differential equations with a delayed argument did not change until the 1990s, when Lehman and Kolmanovskii [54] suggested that interesting results could be obtained if the requirement of the averaged equations to be ODE was relaxed and the presence of variables with delayed arguments was allowed. The mathematical formalization of this approach has been documented by Lehman and Weibel [55] and in successive publications by Lakrib et al. [56,57]. In contrast to the HALE method, the method proposed in 1998 by Lehman and Weibel [55] retains DDE instead of ODE:

$$\begin{aligned} \dot{A} &= \frac{1}{T} \int_0^T f_A(A, A_\tau, \varphi, \varphi_\tau, s) ds + \frac{\sigma^2}{4A} + \frac{\sigma}{\sqrt{2}} \xi_1 \\ &= -\frac{1}{2} \alpha A + \frac{1}{2} A_\tau \cos(\omega\tau + \Delta\varphi_\tau) \operatorname{Re}[\mathcal{Q}(A_\tau)] + \frac{1}{2} A_\tau \sin(\omega\tau + \Delta\varphi_\tau) \operatorname{Im}[\mathcal{Q}(A_\tau)] + \frac{\sigma^2}{4A} + \frac{\sigma}{\sqrt{2}} \xi_1 \\ &= \underbrace{\frac{\beta}{k} \cos(\omega\tau + \Delta\varphi) \frac{\sqrt{k^2 A_\tau^2 + 1} - 1}{kA_\tau}}_{F_{LW}(A, A_\tau, \varphi, \varphi_\tau)} - \frac{1}{2} \alpha A + \frac{\sigma^2}{4A} + \frac{\sigma}{\sqrt{2}} \xi_1 \end{aligned} \quad (19a)$$

$$\begin{aligned} \dot{\varphi} &= \frac{1}{T} \int_0^T f_\varphi(A, A_\tau, \varphi, \varphi_\tau, s) ds + \frac{\sigma}{A\sqrt{2}} \xi_2 \\ &= -\frac{1}{2} \left(\omega - \frac{\omega_0^2}{\omega} \right) + \frac{1}{2} \frac{A_\tau}{A} \cos(\omega\tau + \Delta\varphi_\tau) \operatorname{Im}[\mathcal{Q}(A_\tau)] - \frac{1}{2} \frac{A_\tau}{A} \sin(\omega\tau + \Delta\varphi_\tau) \operatorname{Re}[\mathcal{Q}(A_\tau)] + \frac{\sigma}{A\sqrt{2}} \xi_2 \\ &= \underbrace{-\frac{1}{2} \left(\omega - \frac{\omega_0^2}{\omega} \right) - \beta \sin(\omega\tau + \Delta\varphi) \frac{\sqrt{k^2 A_\tau^2 + 1} - 1}{k^2 A A_\tau}}_{G_{LW}(A, A_\tau, \varphi, \varphi_\tau)} + \frac{\sigma}{A\sqrt{2}} \xi_2 \end{aligned} \quad (19b)$$

where $\Delta\varphi \triangleq \varphi(t) - \varphi(t - \tau)$. In this case, the delayed quantities A_τ and φ_τ are treated as independent from their non-delayed counterparts A and φ .

5.5. The method of Wang and Hu (WH method)

In addition to the HALE and LW approaches, we consider a modified method that can be found in Wang and Hu [58]. This last method was applied on a delayed Van Der Pol oscillator and showed some success in retaining the complex system dynamics in the averaged equations and maintaining at the same time a simpler formulation. In fact, this approach returns averaged equations which are delayed but partially decoupled, differently from the standard LW approach:

$$\begin{aligned}\dot{A} &= \frac{1}{T} \int_0^T f_A(A, A_\tau, \varphi, \varphi_\tau = \varphi, s) ds + \frac{\sigma^2}{4A} + \frac{\sigma}{\sqrt{2}} \xi_1 \\ &= -\frac{1}{2} \alpha A + \frac{1}{2} A_\tau \cos(\omega\tau) \operatorname{Re}[\mathcal{Q}(A_\tau)] + \frac{1}{2} A_\tau \sin(\omega\tau) \operatorname{Im}[\mathcal{Q}(A_\tau)] + \frac{\sigma^2}{4A} + \frac{\sigma}{\sqrt{2}} \xi_1 \\ &= \underbrace{\frac{\beta}{k} \cos(\omega\tau) \frac{\sqrt{k^2 A_\tau^2 + 1} - 1}{k A_\tau}}_{F_{WH}(A, A_\tau)} - \frac{1}{2} \alpha A + \frac{\sigma^2}{4A} + \frac{\sigma}{\sqrt{2}} \xi_1\end{aligned}\quad (20a)$$

$$\begin{aligned}\dot{\varphi} &= \frac{1}{T} \int_0^T f_\varphi(A, A_\tau, \varphi, \varphi_\tau = \varphi, s) ds + \frac{\sigma}{A\sqrt{2}} \xi_2 \\ &= -\frac{1}{2} \left(\omega - \frac{\omega_0^2}{\omega} \right) + \frac{1}{2} \frac{A_\tau}{A} \cos(\omega\tau) \operatorname{Im}[\mathcal{Q}(A_\tau)] - \frac{1}{2} \frac{A_\tau}{A} \sin(\omega\tau) \operatorname{Re}[\mathcal{Q}(A_\tau)] + \frac{\sigma}{A\sqrt{2}} \xi_2 \\ &= -\frac{1}{2} \left(\omega - \frac{\omega_0^2}{\omega} \right) - \underbrace{\beta \sin(\omega\tau) \frac{\sqrt{k^2 A_\tau^2 + 1} - 1}{k^2 A A_\tau}}_{G_{WH}(A, A_\tau)} + \frac{\sigma}{A\sqrt{2}} \xi_2\end{aligned}\quad (20b)$$

In this case, the delay term is maintained in the amplitude A but it is dropped in the phase φ .

5.6. Discussion

In the subsequent parts of the paper, we often refer to these three sets of equations, Eqs. (18)–(20), which we name HALE equations, LW equations and WH equations. One can immediately recognize that the HALE equations are a set of non-delayed differential equations where the amplitude equation is decoupled from the phase equation. The WH equations are delayed, but maintain the independence of the amplitude equation from the phase one. Finally, the LW equations are a set of fully coupled delayed differential equations. In all three cases, the equations are forced by a white noise, therefore they are referred to as stochastic delayed differential equations (SDDE). The reader should notice that the WH and LW formulations reduce to the HALE formulation in case the delay τ is set to 0. Note also that the three sets of equations presented differ only in the flame response term. In each set, the flame response term in the amplitude equation represents the component of the heat release rate in phase with the pressure oscillations, whereas the flame response term in the phase equation represents the component of the heat release rate in quadrature with respect to the pressure oscillations. A summary of the three presented methods is available in Table 1.

Typically, the original method proposed by Hale [49] is preferred for the simplicity of a system of ODEs compared to a system of DDEs. Nevertheless examples exist where the inclusion of delayed terms in the averaged equations has shown better prediction capability: an early work of Wirkus and Rand [59] has been recently revisited by Gluzman and Rand [60] showing improved results when the original averaging method was dropped for the version of Lehman and Weibel [55]. Other researchers (see Sah and Rand [61]) have applied both methods to typical examples of nonlinear equations, i.e. the Duffing and the Van der Pol oscillators, concluding that the performance of the two methods depends on the considered nonlinearity and suggesting to apply the more elaborate LW approach, especially in cases when τ becomes large. So far, in the thermoacoustics community the attempts to introduce a delay in the Galerkin projection Eq. (1) resulted in equations for the amplitude A and the phase φ which were either of the HALE type (see for example Crawford et al. [7,8], where the steady state statistics based on the Fokker–Plank equation suggest non-delayed averaged equations) or of the WH type (e.g. Ghirardo et al. [9]). In this latter case, noisy forcing was not introduced in the dynamics. In the authors' knowledge, the work presented here is the first to discuss a delayed coupled formulation of the LW form for thermoacoustic applications.

In the following Section 6, we discuss the fixed points of the considered three sets of equations and investigate their linear stability. These results are compared with numerical simulations of the original equation in η (Section 7) and allow us to define which of the three sets of equations is a better approximation of the system dynamics and, for example, should be used to perform system identification based on experimental data.

6. Stability of limit-cycle solutions

The averaged equations, Eqs. (18)–(20), introduced in Section 5, exhibit the same fixed points. These are obtained by setting the slowly varying amplitude A and its delayed counterpart A_τ to a mean amplitude \bar{A} and the phases φ and φ_τ to a

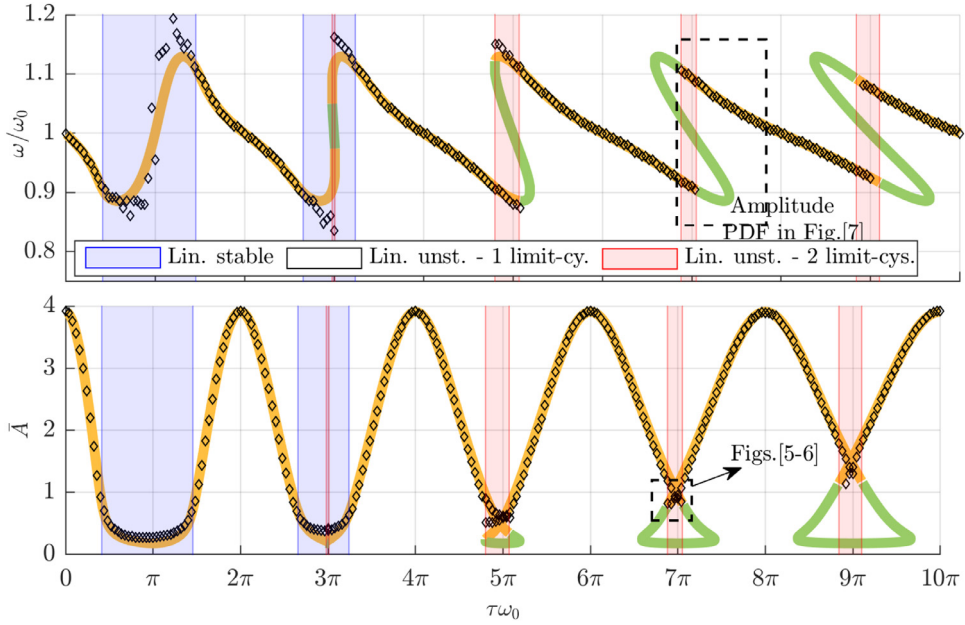


Fig. 4. Yellow and green lines: bifurcation diagram of the delayed thermoacoustic oscillator Eq. (7), i.e. fixed points of the averaged equations Eqs. (18)–(20) obtained as sets of $[\bar{A}, \omega]$ solution of Eq. (21), as function of the normalized delay $\tau\omega_0$. All fixed points are linearly stable for HALE and for WH. In the LW formulation, the yellow lines are linearly stable fixed points, whereas the green lines are linearly unstable. Black diamonds: fixed points as extracted from post-processing of numerical simulations of the delayed thermoacoustic oscillator Eq. (7). Note that for some delays (e.g. $\tau\omega_0 = 7\pi$) two diamonds at different amplitudes and oscillation frequencies are reported. These are bistability conditions where the system randomly switches between two stable fixed points. (For interpretation of the references to color in this figure legend, the reader is referred to the web version of this article.)

mean fast varying phase $\bar{\varphi}$. The time derivatives are set to zero and a system of two coupled nonlinear algebraic equations is obtained:

$$\frac{\beta}{k} \cos(\omega\tau) \frac{\sqrt{k^2\bar{A}^2 + 1} - 1}{k\bar{A}} - \frac{1}{2}\alpha\bar{A} + \frac{\sigma^2}{4\bar{A}} = 0 \tag{21a}$$

$$-\frac{1}{2}\left(\omega - \frac{\omega_0^2}{\omega}\right) - \beta \sin(\omega\tau) \frac{\sqrt{k^2\bar{A}^2 + 1} - 1}{k^2\bar{A}^2} = 0 \tag{21b}$$

It can be noted that Eq. (21) do not depend on the mean fast varying phase $\bar{\varphi}$. Indeed, in the three original systems of equations, Eqs. (18)–(20), the fast varying phase φ never appears separate but always in combination with its delayed counterpart φ_τ in the expression $\Delta\varphi$. This means that the dynamical system is not influenced by the value of φ itself and therefore does not exhibit a preferential value for this quantity [43]. On the other hand, the system of equations Eq. (21) is depending on the unknown quantity ω , the thermoacoustic frequency of oscillation. Previous works [9] have shown how neglecting the shift from the acoustic to the thermoacoustic frequency of oscillation, i.e. the imaginary part of the describing function, can lead to mistakes in assessing the system stability. Therefore, for a given set of parameters α/ω_0 , β/ω_0 , $\tau\omega_0$ and $k\sigma/\sqrt{\omega_0}$, we are looking for the couples $[\bar{A}, \omega]$ that are solutions of Eq. (21). In general, these are multiple.

Combining Eqs. (21a) and (21b) and applying some algebra one obtains an equation in ω only:

$$\beta[(\omega^2 - \omega_0^2) + \beta\omega \sin(\omega\tau)][(\omega^2 - \omega_0^2) \cos(\omega\tau) + \alpha\omega \sin(\omega\tau)] - \frac{1}{8}\sigma^2k^2(\omega^2 - \omega_0^2)^2 = 0 \tag{22}$$

This equation can be solved numerically on the positive real line for an oscillation frequency ω close to the acoustic frequency ω_0 . The corresponding limit cycle amplitude \bar{A} can be obtained from Eq. (21). One notices that imposing the condition $\sigma = 0$ in Eq. (22), i.e. assuming a deterministic framework, results in a condition for ω perfectly equivalent to that presented in Eq. (27) by Ghirardo et al. [9].

Since the main focus of this work is on the effect of the time delay we analyze the fixed points in Eq. (21) parametrically in the delay $\tau\omega_0$, as stated in Section 3. We present in Fig. 4c the result of this analysis. For small delays $\tau\omega_0$, the system Eq. (21) presents a single solution with an oscillation amplitude \bar{A} which is almost periodic in $\tau\omega_0$: when the heat release of the flame is in phase with the acoustics the system is pushed away from the zero amplitude solution and evolves into a limit cycle. This happens cyclically for $\tau\omega_0 = [0, 2\pi, 4\pi, \dots]$. When instead the acoustics and the flame response are in antiphase, the thermoacoustic energy of the system is decreased [5] and the oscillations tend to be damped, $\tau\omega_0 = [\pi, 3\pi, \dots]$.

This establishes an equilibrium with the stochastic forcing and results in a system oscillating at lower amplitudes. Large delay times introduce more equilibria in the system dynamics. A saddle-node bifurcation occurs, for example, slightly before $\tau\omega_0 = 5\pi$ and introduces two additional low-amplitude equilibria. The bifurcation diagram in Fig. 4 clearly shows how two of them coalesce and disappear just after the critical delay $\tau\omega_0 = 5\pi$. The same qualitative behavior is observed also at $\tau\omega_0 = 7\pi$ and $\tau\omega_0 = 9\pi$. For increasing time delays (not presented in Fig. 4), the same behavior would be observed over larger symmetric segments around $\tau\omega_0 = [11\pi, 13\pi, \dots]$. Zones with 5 or more equilibria arise in the system dynamics.

We continue our analysis of Eqs. (18)–(20) performing a linear stability analysis for all fixed points separately. The results of this analysis are different for the three sets of equations presented, Eqs. (18)–(20), and constitute an important benchmark with respect to the numerical simulations of the original equation in η . To perform this stability analysis the stochastic forcing $\xi(t)$ is dropped and the linearization occurs around the fixed points $[A, \varphi] = [\bar{A}, 0]$. The choice of 0 as fixed point for the phase is completely arbitrary and another choice could have been made without affecting the results. The linearized equations are:

$$\dot{A} = \frac{\partial F}{\partial A}(A - \bar{A}) + \frac{\partial F}{\partial A_\tau}(A_\tau - \bar{A}) + \frac{\partial F}{\partial \varphi}\varphi + \frac{\partial F}{\partial \varphi_\tau}\varphi_\tau \tag{23a}$$

$$\dot{\varphi} = \frac{\partial G}{\partial A}(A - \bar{A}) + \frac{\partial G}{\partial A_\tau}(A_\tau - \bar{A}) + \frac{\partial G}{\partial \varphi}\varphi + \frac{\partial G}{\partial \varphi_\tau}\varphi_\tau \tag{23b}$$

The presented equations are general and a different expression is obtained for each choice of the functions $F = F(A, A_\tau, \varphi, \varphi_\tau)$ and $G = G(A, A_\tau, \varphi, \varphi_\tau)$. For example, if F and G are selected as in the HALE formulation (i.e. $F = F_H$ and $G = G_H$), all partial derivatives with respect to delayed quantities (e.g. $\partial/\partial\varphi_\tau$) are identically zero. The eigenvalues are obtained seeking a solution of the form $\mathbf{x} = \mathbf{x}_0 e^{\lambda t}$, where λ is a complex number and \mathbf{x} a vector collection of $A - \bar{A}$ and φ , which results in three characteristic equations for HALE, WH and LW, respectively:

$$\lambda\left(\lambda - \frac{\partial f}{\partial A}\right) = 0 \tag{24a}$$

$$\lambda\left(\lambda - \frac{\partial f}{\partial A} - \frac{\partial f}{\partial A_\tau}e^{-\lambda\tau}\right) = 0 \tag{24b}$$

$$\left(\lambda - \frac{\partial f}{\partial A} - \frac{\partial f}{\partial A_\tau}e^{-\lambda\tau}\right)\left(\lambda - \frac{\partial g}{\partial \varphi} - \frac{\partial g}{\partial \varphi_\tau}e^{-\lambda\tau}\right) - \left(\frac{\partial g}{\partial A} + \frac{\partial g}{\partial A_\tau}e^{-\lambda\tau}\right)\left(\frac{\partial f}{\partial \varphi} + \frac{\partial f}{\partial \varphi_\tau}e^{-\lambda\tau}\right) = 0 \tag{24c}$$

The characteristic equation for the HALE formulation, Eq. (24a), is a second order polynomial; whereas the characteristic equations for the WH and LW formulations, Eqs. (24b) and (24c), are transcendental equations in the complex variable λ . This is expected because Eq. (18) are ordinary differential equations, whereas Eqs. (19) and (20) are delay differential equations and therefore, in general, allow for an infinite number of eigenvalues after being linearized. One notices also that all three characteristic equations Eq. (24) share the solution $\lambda = 0$. This is evident in Eqs. (24a) and (24b), whereas in Eq. (24c) results from the properties $\partial F_{LW}/\partial\varphi = -\partial F_{LW}/\partial\varphi_\tau$ and $\partial G_{LW}/\partial\varphi = -\partial G_{LW}/\partial\varphi_\tau$. The presence of a neutrally stable eigenvalue should not surprise, in fact the dynamics on the φ equation is undetermined (no preferential value for φ). This is reflected in an eigenvalue $\lambda = 0$. In the remainder of this paper, we define a fixed point as asymptotically stable if all its eigenvalues but the one at $\lambda = 0$ have a negative real part.

The stability analysis for the HALE formulation is straightforward since the overall system stability is controlled only by the real part of $\partial F_H/\partial A$. In Fig. 4, all fixed points are asymptotically stable for HALE.

The stability analysis for Eqs. (24b) and (24c) is more elaborate since an infinite number of complex valued eigenvalues needs to be tracked. Fortunately, methods exist in the literature to check the system stability without this direct computation, examples can be found in Insperger and Stépán [39] and Kolmanovskii [62], where many theorems on DDE stability are summarized. Stepan’s method, which is used in Section 4, is an example. The results of the stability analysis show that all fixed points in Fig. 4 are asymptotically stable in the WH formulation, coherently with the analysis performed for HALE. The LW set of equations shows instead that a number of fixed points (green lines in Fig. 4) are unstable, in particular all those in the lower branch of the saddle node bifurcation and some of those in the upper one. This result is in contradiction with the ones for HALE and WH.

Practically, the bifurcation diagram presented in Fig. 4 does not constitute a novelty compared to other analytical [9], numerical [63] and experimental [64] results. Its importance lies in the fact that it allows a comparison between equilibria and stability characteristics of three slow flow equations derived from the same fast flow Eq. (1). This is new because previous investigations [7,9] never discussed different slow flow equations. Additionally, this is significant because it might have practical implications on previous modeling and system identification works [2,4] which a priori assumed HALE-type slow flow equations.

The stability results obtained in this section are valid only for the flame model of Eq. (3). Different flame models will lead to quantitatively different but qualitatively similar results, as long as the shape of the flame describing function Eq. (17) is not significantly modified. For example, the results of this section can change significantly if the flame model allows also for subcritical bifurcations.

7. Comparison with numerical simulations

The analysis in Sections 5 and 6 presents three sets of different slow flow equations which share the same fixed points but have different stability characteristics. In the present section, we benchmark the analytical and numerical results obtained for these three sets of equations, Eqs. (18)–(20), with the numerical simulation of the original system in η , i.e. Eq. (7).

We simulate 200 times Eq. (7) with the parameters fixed as detailed in Section 3 and change the nondimensional delay $\tau\omega_0$ in the range $[0, 10\pi]$. We make use of the numerical scheme of [66,65], which is a modified version of the Euler-Maruyama scheme able to take into account the presence of a delay in the equations. The system is simulated for a sufficiently long time so that the statistics of slowly varying amplitude A are converged. Each simulation is post-processed extracting the slowly varying amplitude A and phase φ of oscillation, alongside with the thermoacoustic frequency ω . Details on the procedures can be found in other works [19,67,68].

We present in Fig. 4 the fixed points as extracted from the time domain simulations in η (black diamonds) and the analytical results from Section 6 (yellow and green lines). For small time delays $\tau\omega_0$, the system presents a unique stable fixed point and this matches with great accuracy with the conclusions drawn in Section 6. For larger delays, when multiple fixed points arise, i.e. in the regions around $\tau\omega_0 = [5\pi, 7\pi, 9\pi, \dots]$, the simulated system in η does not oscillate at a single frequency ω but switches randomly among two different frequencies ω . This is related to the presence of two stable limit cycles. The presence of noise exciting the system explains the random switches between the two, characterized by two different sets $[\bar{A}, \bar{\omega}]$. These results are coherent with the LW formulation, predicting two closely spaced fixed points at the indicated amplitude and frequency. This behavior is frequently observed in thermoacoustics [6,25].

In Fig. 5 we focus on conditions featuring multiple stable limit cycles, presenting different spectra of η simulated with $\tau\omega_0 = [6.88\pi, 6.92\pi, 6.96\pi, 7.00\pi, 7.04\pi]$. Additionally, we present two dimensional probability density functions for the instantaneous frequency and amplitude of oscillation. In all five simulations, the dynamical system of Eq. (7) is stochastically switching between a frequency smaller than ω_0 (blue cross) and a frequency larger than ω_0 (red cross). The preference for one of the two states with respect to the other depends on the time delay $\tau\omega_0$. In this case, delays smaller than $\tau\omega_0 = 6.96\pi$ favor the low frequency oscillation (and vice versa). This behavior can be explained by considering the phase equation in the LW formulation, i.e. Eq. (19b). The driving stochastic term $\sigma/(A\sqrt{2})\xi_2$ is divided by the amplitude of oscillation and, for example for $\tau\omega_0 = 6.88\pi$, this amplitude is larger for the low frequency fixed point, implying a smaller effective noise intensity $\sigma/(\sqrt{2}A)$ when the system lingers at this condition. For a smaller noise intensity, it is more difficult for the system to switch to a different fixed point, explaining why the dynamical system prefers one stable stochastic attractor to the other.

Three additional plots are reported in Fig. 6 for the $\tau\omega_0 = 6.96\pi$ case. They show how bistability is evident from the time domain (left), the frequency domain (right, spectrogram), and from the post-processed slowly varying quantities (middle).

Analogous results to those presented in Figs. 5 and 6 can be derived if Eq. (19) are simulated directly. Indeed, the dynamical system as written in Eq. (19) can automatically modify its frequency of oscillation ω : a solution of the type $[A, \varphi] = [\bar{A}, Kt]$ with K constant can arise. The system switches from a frequency ω to a different one, $\omega + K$, which becomes a new fixed point. The equations written in the LW formulation exhibit this great advantage: even if the imposed

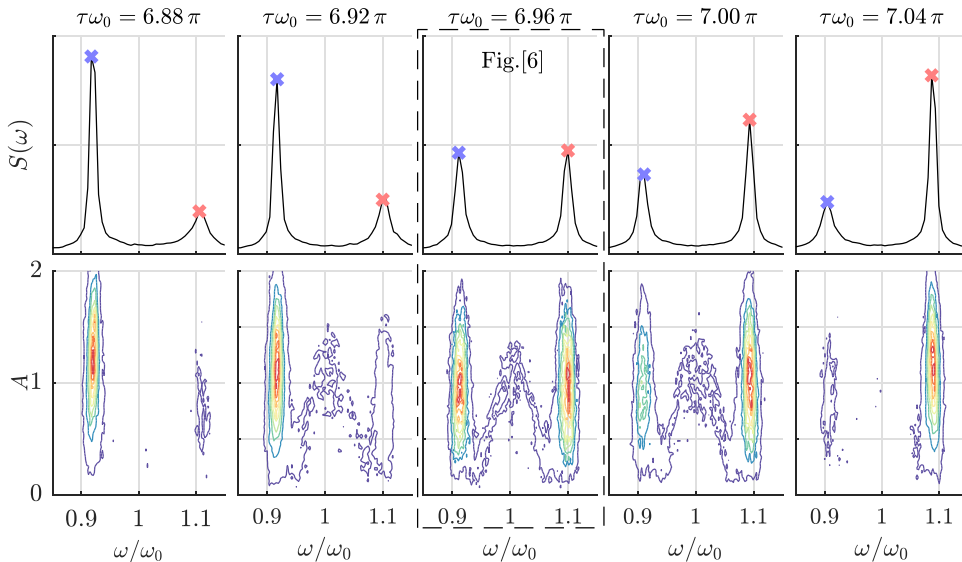


Fig. 5. Examples of bistability from simulations of the thermoacoustic oscillator of Eq. (7). Top: power spectral density of η for five different simulations of Eq. (7), from left to right $\tau\omega_0 = [6.88\pi, 6.92\pi, 6.96\pi, 7.00\pi, 7.04\pi]$, other parameters as defined in Section 3. Bottom: joint probability density function of (A, ω) . Fig. 6 presents results from the middle plot simulation ($\tau\omega_0 = 6.96\pi$). All five reported simulations oscillate at two distinct frequencies. As the bifurcation parameter $\tau\omega_0$ is increased, the statistical preference of the system switches from the lower frequency to the higher frequency oscillation.

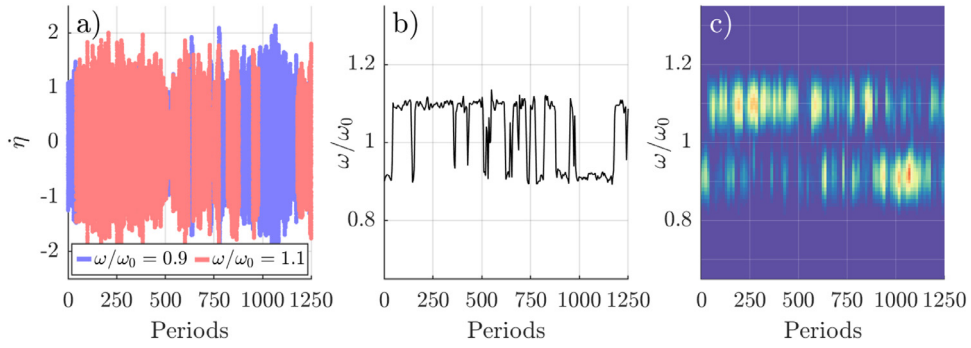


Fig. 6. Example of bistability from simulation of the thermoacoustic oscillator Eq. (7). Left (a): time domain of η colored by oscillation frequency ω . Middle (b): oscillation frequency as slope of $\phi(t) = \omega t + \varphi$. Right (c): spectrogram of η . Plots referred to the case $\tau\omega_0 = 6.96\pi$, also reported in Fig. 5.

value of ω is not corresponding to that of a fixed point $[\bar{A}, \omega]$, the dynamical system can correct this converging to a solution $[A, \varphi] = [\bar{A}, Kt]$, where $K + \omega$ is the correct frequency of oscillation. This feedback mechanism is related to the presence of the $\Delta\varphi$ term, which results in the fact that the amplitude equation is coupled to the phase one and therefore sensitive to trends in the phase φ .

The HALE and WH formulations fail due to two reasons: firstly, they predict a third stable fixed point (purple line in Fig. 4), which is never observed in the original η system, Eq. (7). Secondly, they are not able to capture such rich dynamics: simulating Eqs. (18) or (20) with an initial value of the amplitude close to \bar{A} and an oscillation frequency ω given by the fixed point value results in a time series $[A(t), \varphi(t)]$ staying close to the fixed point, but never switching between two of them. Additionally, if the imposed ω is not the correct one, the system will converge to a wrong status.

8. Statistics of the slowly varying amplitude A

As presented in other works [2,4,43], the distribution of the slowly varying amplitude A is often used to extract meaningful information of the original dynamical system of Eq. (7). We review in Section 8.1 the main results available in the literature, introduce a new formulation in Sec. 8.2, and compare both of them with simulations of Eq. (7) in Section 8.3.

8.1. Probability density function of the amplitude A as in the HALE formulation

The slowly varying amplitude A in the case of a non-delayed flame model [4] or in a HALE formulation (Eq. (20)) is governed by a stochastic differential equation decoupled from the phase equation, see for example [2]. The equation can be written in the form:

$$\dot{A} = F(A) + \frac{\sigma}{\sqrt{2}}\xi_1 \quad (25)$$

where the unspecified function $F(A)$ contains the information relative to the nonlinearity of the flame response in Eq. (2). The evolution of the probability density function $P(A, t)$ of the amplitude A with the time t is governed by a Fokker-Planck equation [45,53], which in the stationary case simplifies to an ordinary differential equation:

$$0 = -\frac{d}{dA}[F(A)P(A)] + \frac{\sigma^2}{4} \frac{d^2P}{dA^2} \quad (26)$$

The solution is given by:

$$P(A) = C \exp\left(\frac{4}{\sigma^2} \int F(A') dA'\right) \\ \text{with } C \text{ so that } \int_0^\infty P(A) dA = 1 \quad (27)$$

This result was presented already in the early 2000's by Lieuwen [43] and has been used in a system identification perspective with a gray box model for $F(A)$ by Noiray and Schuermans [4] and with a black box model by Ghirardo et al. [2]. With the current assumption of the nonlinear term in Eq. (3), the explicit expression of the probability density function of Eq. (27) in the HALE formulation becomes:

$$P(A) = CA \exp\left\{\left(\frac{4\beta}{k^2\sigma^2} \cos(\omega\tau) [\sqrt{(1+k^2A^2)} - \log(1 + \sqrt{(1+k^2A^2)})] - \frac{\alpha}{\sigma^2} A^2\right)\right\} \\ \text{with } C \text{ so that } \int_0^\infty P(A) dA = 1 \quad (28)$$

8.2. Probability density function of the amplitude A as in the WH formulation

In case one decides to opt for a formulation of the slowly varying equations of WH-type, the expression of Eq. (28) is not valid anymore. Indeed, the time evolution of the amplitude is governed by a stochastic delay differential equation, Eq. (20a):

$$\dot{A} = \frac{\beta}{k} \cos(\omega\tau) \frac{\sqrt{k^2 A_\tau^2 + 1} - 1}{k A_\tau} - \frac{1}{2} \alpha A + \frac{\sigma^2}{4A} + \frac{\sigma}{\sqrt{2}} \xi_1 \quad (20a)$$

The Fokker–Planck equation as introduced in Roberts and Spanos [45] is not anymore applicable because of the delayed term A_τ . Besides relying on direct numerical simulations, perturbation methods exist to recast the closed-form expression of $P(A)$ [69–72]. Different works have shown the applicability of these expansions techniques to SDDE in biology, and other sciences. In the present discussion, we build upon the work of Frank [69] who presents a perturbation method applicable to nonlinear stochastic systems with time delay. The key assumption is that the delay τ weakly interacts with the system dynamics. A detailed derivation is presented in the Appendix A. The first-order approximation of the probability density function is:

$$P^{(1)}(A) = CA \exp \left\{ \left(-\frac{4}{\sigma^2} \left[\left(\frac{\sigma^2}{4A} - Kc_2 \right) (A - \bar{A}) - \frac{1}{2} (c_1 + 3Kc_3) (A - \bar{A})^2 e^{-\frac{\sigma}{2}\tau} + \dots \right. \right. \right. \\ \left. \left. \left. \dots + \frac{1}{4} \alpha (A - \bar{A})^2 - \frac{c_2}{3} (A - \bar{A})^3 e^{-\alpha\tau} - \frac{c_3}{4} (A - \bar{A})^4 e^{-\frac{3}{2}\alpha\tau} \right] \right) \right\} \quad (29)$$

where the constants c_1 , c_2 and c_3 are explicitly reported in Appendix A, K is defined as $K = \sigma^2 / (2\alpha)(1 - \exp(-\alpha\tau))$ and C is chosen such that the area under the distribution is unitary. We remark that Eq. (29) reduces to Eq. (28) if the delay τ is set to zero and the nonlinear term in Eq. (28) is expanded in series; Eq. (28) can be therefore seen as a particular case of Eq. (29) when the delay τ is small.

8.3. Comparison against numerical simulations

The two analytical expressions of the PDF of the amplitude, Eqs. (28) and (29), are compared with the numerical probability density function obtained solving the original Eq. (7) for the time evolution of η (ground truth). The results are presented for six different delays $\tau\omega_0$ in Fig. 7, where additionally the amplitude PDF from the numerical solutions of the HALE, WH and LW systems of equations, Eqs. (18)–(19), are depicted.

We first remark the perfect match between the numerical PDFs obtained from the η simulations (ground truth) and the LW formulation for all delays $\tau\omega_0$. This is crucial and confirms the correctness of the LW set of Eq. (19). As is apparent from Fig. 7 and will be even more from Fig. 8, the same cannot be concluded for HALE and WH formulations. In particular, the HALE formulation, Eq. (18), is found to perform poorly for all delays $\tau\omega_0$, whereas the WH approach, Eq. (20), is able to capture the system dynamics when the acoustics is in phase with the flame response. Indeed, these conditions, which are in practice the most relevant ones, are characterized by a limited coupling between the amplitude and phase equation and the LW set of equations Eq. (19) is well approximated by the WH approach Eq. (20).

From Fig. 7, the performance of the standard small delay approximation PDF, Eq. (28), can be evaluated. The distance between the prediction and the target PDF is large for all delays $\tau\omega_0$, showing a slightly better behavior for in phase conditions. On the contrary, the perturbation-method PDF (Frank), Eq. (29), behaves better and outperforms Eq. (28) for almost all delays. As expected, its performance drops when the flame and the acoustics are out of phase since neglecting the $\Delta\varphi$ coupling in the amplitude equation is not anymore justified.

We make use of the Hellinger distance to quantify the accuracy of the three sets of equations, HALE, WH and LW, and of the two analytical formulations in reproducing the amplitude PDF over the larger set of delays $[0, 10\pi]$. Given two probability density functions $f(x)$ and $g(x)$, the Hellinger distance $H(f, g)$ is a measure of their distance defined as:

$$H^2(f, g) = 1 - \int_{\Omega} \sqrt{f(x)g(x)} dx \quad (30)$$

where Ω is the common domain of definition of $f(x)$ and $g(x)$. The distance $H(f, g)$ satisfies the condition $0 \leq H(f, g) \leq 1$, the equality $H(f, g) = 0$ holds only if $f(x) \equiv g(x)$, whereas $H(f, g) = 1$ is obtained when $f(x)$ and $g(x)$ never overlap in Ω .

We compute the Hellinger distance between the amplitude PDF obtained from post-processing numerical simulations of $\eta(t)$ and each of the five other PDFs we introduced, namely the three numerical results from the integration of Eqs. (18)–(20) (HALE, WH and LW, respectively), and the two analytical expressions Eqs. (28) and (29). The results are presented in Fig. 8 for $\tau\omega_0 \in [0, 10\pi]$.

The results for the LW formulation (yellow circles) are outstanding over the entire parameter space, confirming again that this set of equations is the most accurate in reproducing the fast dynamics of the original system in η . All other formulations perform poorly in the vicinity of $\tau\omega_0 = [\pi, 3\pi, 5\pi, \dots]$ and present different degrees of accuracy at other values of $\tau\omega_0$. In particular, all formulations tend to collapse when the delay $\tau\omega_0$ approaches 0, as expected. On the other side of the spectrum, for large $\tau\omega_0$, the non-delayed formulations, HALE and Eq. (28) (crosses), show a significant loss of accuracy compared to the formulations that retain delayed information A_τ and φ_τ . Note also that the purple crosses

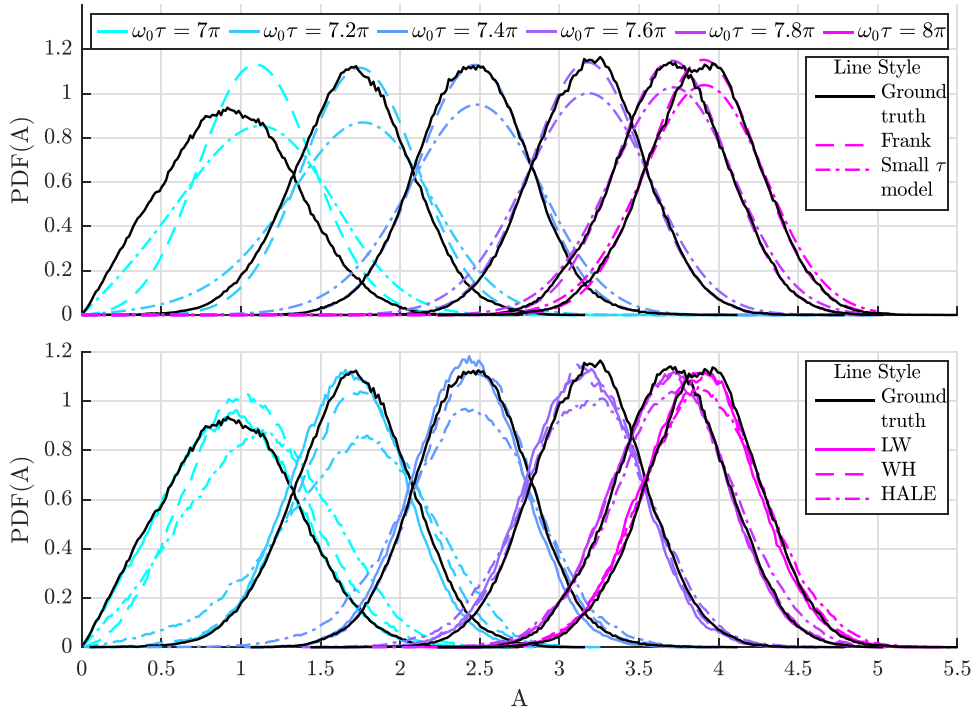


Fig. 7. Probability density function of the amplitude of oscillation A for 6 different delays $\tau\omega_0$. Top plot: comparison between the amplitude extracted from numerical simulation of η , Eq. (7) (ground truth), and two analytical models. Colored dashed line: Frank perturbation model Eq. (29). Colored dash-dotted line: small delay model Eq. (28). Bottom plot: comparison between the amplitude extracted from numerical simulation of η , Eq. (7) (ground truth), and numeric simulations of three models. Colored solid line: LW model, Eq. (19). Dashed line: WH model, Eq. (20). Dash-dotted line: HALE model, Eq. (18). The accuracy of the LW model is remarked over all delays $\tau\omega_0$. The line style of the lines in the top and in the bottom frame has been chosen to mirror connections between the plotted PDFs. In particular, the dashed line in the top frame (Frank) is the result of the analytical solution of the WH equations (dashed line in the bottom frame). The same holds for the pair small delay model - HALE (dash-dotted).

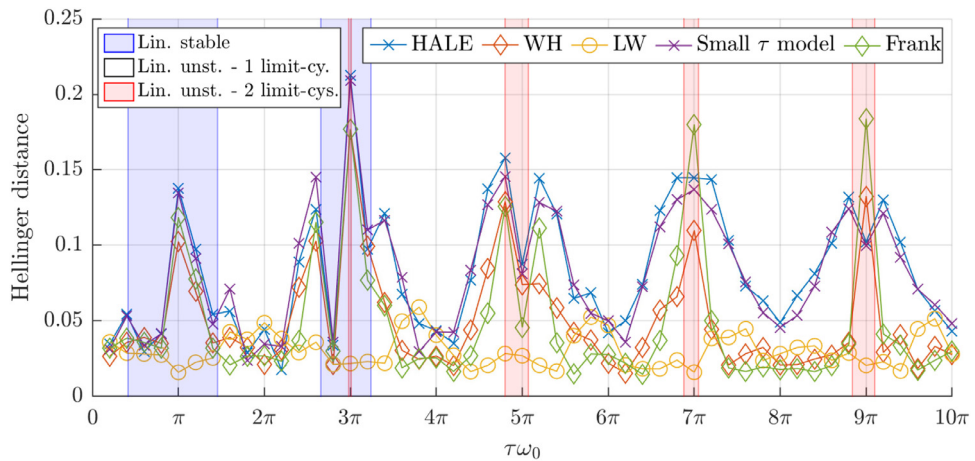


Fig. 8. Hellinger distance between the probability density function of the amplitude A extracted from numerical simulations of Eq. (7) in η (ground truth) and different other PDFs (top right legend). HALE, WH and LW refer to the different averaging models introduced, in particular the PDFs are obtained from numerical simulations of Eqs. (18)–(19) respectively. Small τ model and Frank refer to two analytical approximations of the amplitude PDFs, Eqs. (28) and (29). The LW model is the only one with a good performance over all delays $\tau\omega_0$. Among the analytical models, Frank perturbation method is accurate for all in phase conditions. All models behave similarly in the limit $\tau\omega_0 \rightarrow 0$. Related methods (e.g. WH - Frank) are presented with the same symbol but different color.

(Eq. (28)) closely follow the blue crosses (HALE), in accordance with the fact that Eq. (28) has been obtained as analytical solution of Eq. (18) in the HALE formulation. In the same manner and for the same reason, the green diamonds (Frank) behave similarly to the red diamonds (WH). To obtain an analytical expression with good performance also for the out of phase conditions one needs a PDF approximation for the LW formulation, which naturally implies that a fully coupled phase equation has to be retained. This analytical approximation can be obtained following the generalization of the perturbation method applied in Section 8.2 to multivariate stochastic processes. The necessary theoretical framework is derived in the work of Frank [71], to where we redirect an interested reader.

The results presented in this section have a significant impact on amplitude-based system identification procedures [2,4]. In fact, identified growth rates and other parameters can be substantially different from the exact values if the thermoacoustic cycle contains delays that cannot be considered as short. For example, from inspection of Fig. 8, it is evident that for most values of $\tau\omega_0$ a HALE-based amplitude PDF system identification approach (blue line) is bounded to large errors.

9. Statistics of the slowly varying phase

Information regarding the noise intensity level are embedded in the statistics of the slowly varying phase $\varphi(t)$ [4]. In particular, often the phase equation is reduced to a Wiener process [2,35]:

$$A\dot{\varphi} = \frac{\sigma}{\sqrt{2}}\xi \tag{31}$$

The underlying hypothesis is that the deterministic term $G_{LW}(A, A_\tau, \varphi, \varphi_\tau)$ in Eq. (19) is zero at the $[\bar{A}, \bar{\omega}]$ limit-cycle solution, as per Eq. (21). If Eq. (31) holds, the process $A\dot{\varphi} \sim N(0, \sigma^2/2)$, where $N(M, \Sigma^2)$ denotes a normal distribution of mean value M and variance Σ^2 . The validity of Eq. (31) in describing the dynamics of the slowly varying phase has been successfully verified for a non-delayed flame model [4]. In Fig. 9, we present the standard deviation of $A\dot{\varphi}$ versus the flame delay $\tau\omega_0$. Note that each point presented in Fig. 9 has been obtained from the post-processing of the corresponding fast varying variable $\dot{\eta}(t)$. The probability density function for each point of Fig. 9 is not presented explicitly. It has, however, been verified that each one is normally distributed applying the one-sample Kolmogorov-Smirnov test for Gaussianity with a significance level $\alpha = 0.01$. The test has failed only for two cases, $\tau\omega_0 = 7\pi$ and $\tau\omega_0 = 9\pi$; for these points two equally important oscillation frequencies exist and the PDF is bimodal.

It is apparent that, beside at the limit for small delays $\tau\omega_0 \rightarrow 0$, none of the distributions, although being Gaussian, presents the theoretical variance $\sigma^2/2$ as per Eq. (31). In particular, the errors can be as large as 100% and no conclusion can be made about the error sign, with out of phase conditions featuring larger variances and in phase conditions featuring smaller ones. The reason behind the presented mismatch is the G_{LW} term in Eq. (19) being zero just at the exact fixed point conditions, deviating from this due to the dynamic nature of the amplitude process $A(t)$ and of the phase difference process $\Delta\varphi(t)$.

A verification has been carried out on the statistics of the slowly varying phase φ , which has been found to be uniformly distributed for all studied conditions. This is in accordance with the equations derived in this manuscript, Eq. (19). Indeed, no direct dependence from the phase φ is found, but just from its increment $\Delta\varphi$. Therefore, no preferential value for φ is expected.

The present section has to be carefully considered when predicting and/or recovering noise information from the process $A\dot{\varphi}$, because this can lead to large over- and underestimation of the correct value of σ . On the basis of the results presented in Fig. 8 for the amplitude PDF and on those in Fig. 9 for the $A\dot{\varphi}$ process PDF, we conclude that small-delay models, like Eqs. (28) and (31), based on a HALE formulation, can be considered accurate up to a delay $\tau\omega_0 = \pi/2$, i.e. up to delays 4 times smaller than an acoustic period.

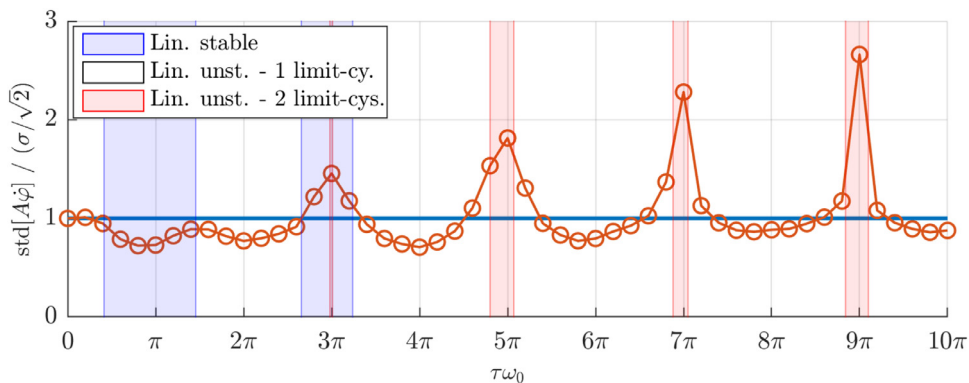


Fig. 9. Ratio between the standard deviation of the process $A\dot{\varphi}$ recovered from simulations of η , Eq. (7), and $\sigma/\sqrt{2}$, standard deviation of the white noise forcing Eq. (31). In the limit for $\tau\omega_0 \rightarrow 0$ the two quantities coincide. This plot shows that Eq. (31), commonly used in thermoacoustic applications, is accurate only for small delays τ , i.e. approximately $\tau\omega_0 < \pi/2$.

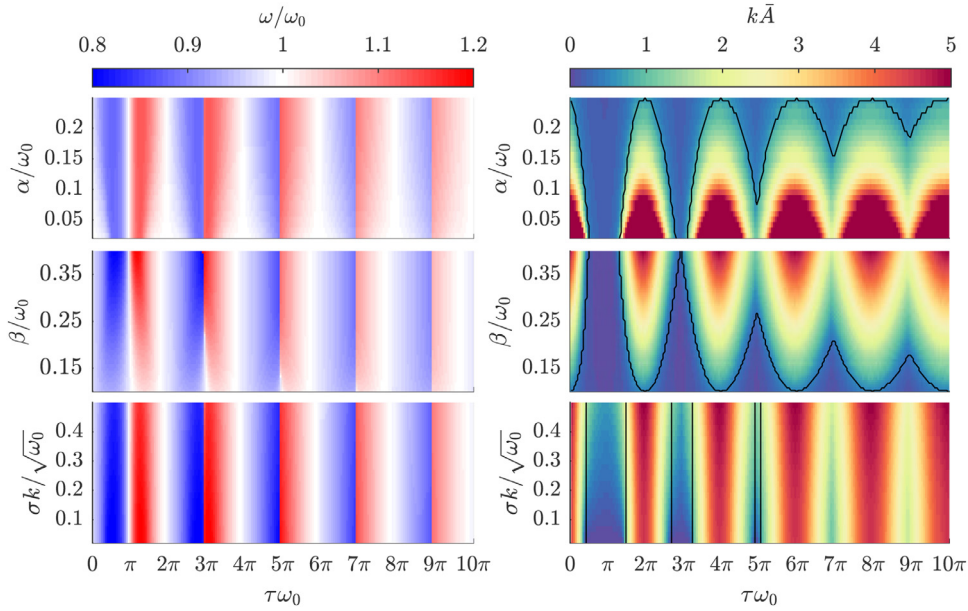


Fig. 10. Mean normalized oscillation frequency $\bar{\omega}/\omega_0$ and amplitude $k\bar{A}$ as function of the nondimensional delay $\tau\omega_0$ and of three parameters: the damping coefficient α/ω_0 , the flame strength β/ω_0 and the noise intensity $k\sigma/\sqrt{\omega_0}$. In each plot one of the parameters is varied keeping the other two constants (base values: $\alpha/\omega_0 = 0.1$, $\beta/\omega_0 = 0.25$, $k\sigma/\sqrt{\omega_0} = 0.15$). The black contour line on the amplitude plots encases regions of linear stability (blue). (For interpretation of the references to color in this figure legend, the reader is referred to the web version of this article.)

10. Effect of parameters variation

Throughout the manuscript the parameter values in the model of Eq. (7) are kept constant to better focus on the effect of the time delay $\tau\omega_0$. In particular, the nondimensional flame strength is set to $\beta/\omega_0 = 0.25$, the damping coefficient to $\alpha/\omega_0 = 0.1$, and the noisy intensity level to $k\sigma/\sqrt{\omega_0} = 0.15$. In the current section we relax these constraints and show that variations of these parameters modify quantitatively, but not qualitatively, the oscillator behavior. We present in Fig. 10 the normalized limit-cycle amplitude $k\bar{A}$ and frequency $\bar{\omega}/\omega_0$ of oscillation³ as function of the nondimensional delay $\tau\omega_0$ and of one among the nondimensional parameters α/ω_0 , β/ω_0 and $k\sigma/\sqrt{\omega_0}$.

Increasing the damping α/ω_0 from its initial condition $\alpha/\omega_0 = 0.1$ results in smaller oscillation amplitudes $k\bar{A}$ and larger linearly stable regions, the opposite is true when the damping is reduced. The effect of the flame strength β/ω_0 is opposite to that of the damping, with large values favoring linearly unstable behaviors and large limit-cycle amplitudes. Finally, the system appears quite robust to variations in the noise intensity $k\sigma/\sqrt{\omega_0}$. Indeed, the level of noise is not largely affecting the mean oscillation conditions but the variations from these mean conditions, and this effect cannot be appreciated from Fig. 10.

Focusing on the oscillation frequency ω/ω_0 , a common trend can be observed from the results shown in Fig. 10: the oscillation frequency is largely depending on the delay, whereas the influence of the other parameters appears to be small. In particular, the in phase conditions $\tau\omega_0 = [0, 2\pi, 4\pi, \dots]$ are always oscillating at the acoustic frequency ω_0 , with smaller delays always featuring larger ω (red) and larger delays presenting smaller ω (blue). This is true in the whole parameters space. For the out of phase conditions, $\tau\omega_0 = [\pi, 3\pi, 5\pi, \dots]$, two possibilities are observed. In most cases, the system is oscillating at a smaller than ω_0 frequency for slightly smaller delays (blue) and suddenly switches to a larger than ω_0 frequency (red) once the threshold $\tau\omega_0 = [3\pi, 5\pi, 7\pi, \dots]$ is surpassed. These regions present multiple stable limit-cycle conditions $[\bar{A}, \bar{\omega}]$ and the figures show the moment at which the amplitude of the limit-cycle at larger ω (red) overcomes the amplitude of the limit-cycle at smaller ω (blue) and becomes the dominant phenomenon observed.

Note that another possibility for the out of phase conditions exists. This can be observed for $\tau\omega_0 = \pi$ in all three subfigures and is, specifically for the β/ω_0 case, also observed at $\tau\omega_0 = 3\pi$ and at $\tau\omega_0 = 5\pi$. In this case, the system oscillates at the acoustic frequency ω_0 and, in contrast to the in phase conditions, it separates on the left low oscillation frequencies (blue) and on the right large ones (red). Focusing on the β/ω_0 case, it can be appreciated that for $\tau\omega_0 = 3\pi$ and $\tau\omega_0 = 5\pi$ there is a smooth transition from this last possibility to the first one. Moving vertically at constant $\tau\omega_0$, as the flame strength β/ω_0 is increased, the stable fixed point at $\omega/\omega_0 = 1$ undergoes a supercritical pitchfork bifurcation becoming unstable. Two new stable fixed points are created, of which only the one at $\omega/\omega_0 > 1$ (red) can be observed, because it is the one statistically preferred by the system oscillations.

³ Some of the presented results oscillate at multiple $[\bar{A}, \bar{\omega}]$. In those cases the largest \bar{A} and the corresponding $\bar{\omega}$ are presented.

11. Conclusions

In the present work, the effect of a time delay in modeling thermoacoustic modes with noise has been studied numerically and analytically. To the best of the authors' knowledge, this is the first study combining a nonlinear flame model with a delayed acoustic feedback and stochastic background forcing. This extends and completes different works dealing just with two of these three aspects at a time [4,7,9].

The introduction of a delayed flame model in the standard one-mode Galerkin projection oscillator modifies the classical results based on the study of the slowly varying amplitude A and phase φ . In particular, the widely-used cubic nonlinear saturation function is found to be inadequate, since the delayed feedback of the acoustics on the flame response can trigger diverging solutions. An arctangent model is proposed instead and utilized successfully. Additionally, the standard stochastic averaging method [45] cannot be directly applied due to the presence of a delay τ . Three different methodologies for averaging delayed differential equations are presented and applied resulting in three different sets of slow flow equations, Eqs. (18)–(20). Based on an analytical study and a comparison with numerical results from the original time series in η , we conclude that the method by Lehman and Weibel [55] should be considered when dealing with thermoacoustic systems exhibiting a delay. Only in the particular situation $\tau\omega_0 \ll 2\pi$, the HALE standard formulation can be used instead. This is verified in terms of stability of limit-cycle solutions (Section 6), the capability of the LW equations to reproduce bistability (Section 6), and in terms of statistics on the slowly varying amplitude (Section 8) and phase (Section 9). The implications of these results in studying and identifying thermoacoustic systems are significant because the classical approaches [2,4,43], which are based on non-delayed formulations, fall somewhat short when a delay $\tau\omega_0$ larger than a fraction ($\approx 1/4$) of a limit-cycle 2π is considered.

Additionally, this paper presents how the contribution of intrinsic thermoacoustic modes on the system dynamics is retained if a delayed flame model is chosen over a non-delayed one. This joins the studies on the recently-discovered ITA modes with the traditional Galerkin projection of thermoacoustic modes onto acoustic ones.

Declaration of Competing Interest

The authors declare that they have no known competing financial interests or personal relationships that could have appeared to influence the work reported in this paper.

CRedit authorship contribution statement

Francesco Gant: Conceptualization, Methodology, Software, Validation, Formal analysis, Investigation, Writing - original draft, Writing - review & editing. **Giulio Ghirardo:** Conceptualization, Methodology, Formal analysis, Writing - review & editing, Supervision. **Mirko R. Bothien:** Conceptualization, Writing - review & editing, Supervision, Project administration.

Acknowledgments

This project has received funding from the European Union's [Horizon 2020](#) research and innovation programme under the Marie Skłodowska-Curie grant agreement no. [765998](#), ANNULIGHT.

Appendix A. Amplitude probability density function derivation

We present a detailed derivation of Eq. (29). The nomenclature in this appendix is consistent to the one the reader can find in the original publication of Frank [69], to which we address for more details regarding the theoretical aspects of the perturbation method.

Assuming the system is oscillating at a limit cycle mean amplitude \bar{A} , the amplitude equation Eq. (20a) can be written as:

$$\dot{A} = F^{(0)}(A) + F^{(1)}(A, A_\tau) + \frac{\sigma}{\sqrt{2}}\xi \quad (\text{A.1a})$$

$$F^{(0)}(A) \triangleq -\frac{1}{2}\alpha(A - \bar{A}) \quad (\text{A.1b})$$

$$F^{(1)}(A, A_\tau) \triangleq \frac{\beta}{k} \cos(\omega\tau) \frac{\sqrt{k^2 A_\tau^2 + 1} - 1}{k A_\tau} - \frac{\beta}{k} \cos(\omega\tau) \frac{\sqrt{k^2 \bar{A}^2 + 1} - 1}{k \bar{A}} + \frac{\sigma^2}{4A} - \frac{\sigma^2}{4\bar{A}} \quad (\text{A.1c})$$

where $F^{(0)}(A) + F^{(1)}(A, A_\tau) = F(A, A_\tau)$ because the additional terms in Eqs. (A.1b) and (A.1c) sum up to zero by definition of limit cycle. $F^{(0)}(A)$ is the drift term of the unperturbed system and $F^{(1)}(A, A_\tau)$ represents the perturbation. We consider first the unperturbed problem:

$$\frac{d(A - \bar{A})}{dt} = -\frac{1}{2}\alpha(A - \bar{A}) + \frac{\sigma}{\sqrt{2}}\xi \quad (\text{A.2})$$

Eq. (A.3) is a linear stochastic differential equation for which the transition probability $P^{(0)}(A', t'|A, t)$ is known [69]:

$$P^{(0)}(A', t'|A, t) = \sqrt{\frac{1}{2\pi K(t' - t)}} \exp\left(\frac{[A' - Ae^{-\frac{\alpha}{2}(t' - t)}]^2}{2K(t' - t)}\right)$$

$$K(t' - t) = \frac{\sigma^2}{2\alpha}[1 - \exp -\alpha(t' - t)] \tag{A.3}$$

We expand in series the delayed part of the drift term perturbation $F^{(1)}(A, A_\tau)$:

$$F^{(1)}(A, A_\tau) = \frac{\sigma^2}{4A} - \frac{\sigma^2}{4\bar{A}} + \left.\frac{\partial F^{(1)}(A, A_\tau)}{\partial A_\tau}\right|_{(\bar{A}, \bar{A})} (A_\tau - \bar{A}) + \dots$$

$$\dots + \frac{1}{2} \left.\frac{\partial^2 F^{(1)}(A, A_\tau)}{\partial A_\tau^2}\right|_{(\bar{A}, \bar{A})} (A_\tau - \bar{A})^2 + \frac{1}{6} \left.\frac{\partial^3 F^{(1)}(A, A_\tau)}{\partial A_\tau^3}\right|_{(\bar{A}, \bar{A})} (A_\tau - \bar{A})^3 + \text{h.o.t.}$$

$$\approx -\frac{\sigma^2}{4} \frac{A - \bar{A}}{A\bar{A}} + c_1(A_\tau - \bar{A}) + c_2(A_\tau - \bar{A})^2 + c_3(A_\tau - \bar{A})^3 \tag{A.4}$$

where the constants c_1 , c_2 and c_3 are defined as:

$$c_1 \triangleq \left.\frac{\partial F^{(1)}(A, A_\tau)}{\partial A_\tau}\right|_{(\bar{A}, \bar{A})} = \frac{\beta}{k} \cos(\omega\tau) \frac{(k^2\bar{A}^2 + 1)^{1/2} - 1}{k\bar{A}^2(k^2\bar{A}^2 + 1)^{1/2}} \tag{A.5a}$$

$$c_2 \triangleq \frac{1}{2} \left.\frac{\partial^2 F^{(1)}(A, A_\tau)}{\partial A_\tau^2}\right|_{(\bar{A}, \bar{A})} = \frac{1}{2} \frac{\beta}{k} \cos(\omega\tau) \frac{3k^2\bar{A}^2 - 2(k^2\bar{A}^2 + 1)^{3/2} + 2}{k\bar{A}^3(k^2\bar{A}^2 + 1)^{3/2}} \tag{A.5b}$$

$$c_3 \triangleq \frac{1}{6} \left.\frac{\partial^3 F^{(1)}(A, A_\tau)}{\partial A_\tau^3}\right|_{(\bar{A}, \bar{A})} = \frac{1}{6} \frac{\beta}{k} \cos(\omega\tau) \frac{-3(4k^4\bar{A}^4 + 5k^2\bar{A}^2 - 2(k^2\bar{A}^2 + 1)^{5/2} + 2)}{k\bar{A}^4(k^2\bar{A}^2 + 1)^{5/2}} \tag{A.5c}$$

Building on the work of Frank [69], we need to evaluate the delayed induced drift:

$$\tilde{F}^{(1)}(A) = \int_0^{+\infty} F^{(1)}(A, A_\tau) P^{(0)}(A_\tau|A) dA_\tau$$

$$= \int_0^{+\infty} \sqrt{\frac{1}{2\pi K(\tau)}} F^{(1)}(A, A_\tau) \exp\left(\frac{[A_\tau - Ae^{-\frac{\alpha}{2}\tau}]^2}{2K(\tau)}\right) dA_\tau$$

$$= -\frac{\sigma^2}{4\bar{A}} \frac{A - \bar{A}}{A} + Kc_2 + (c_1 + 3Kc_3)(A - \bar{A})e^{-\frac{\alpha}{2}\tau} + c_2(A - \bar{A})^2 e^{-\alpha\tau} + c_3(A - \bar{A})^3 e^{-\frac{3}{2}\alpha\tau} \tag{A.6}$$

the unperturbed potential:

$$V^{(0)}(A) = -\int F^{(0)}(A) dA = \int \frac{1}{2} \alpha (A - \bar{A}) dA =$$

$$= \frac{1}{4} \alpha (A - \bar{A})^2 \tag{A.7}$$

and the perturbed one:

$$\tilde{V}^{(1)}(A) = -\int \tilde{F}^{(1)}(A) dA = +\frac{\sigma^2}{4\bar{A}} (A - \bar{A} \log A) - Kc_2(A - \bar{A}) + \dots$$

$$\dots - \frac{1}{2} (c_1 + 3Kc_3)(A - \bar{A})^2 e^{-\frac{\alpha}{2}\tau} - \frac{c_2}{3} (A - \bar{A})^3 e^{-\alpha\tau} - \frac{c_3}{4} (A - \bar{A})^4 e^{-\frac{3}{2}\alpha\tau} \tag{A.8}$$

with $K = \sigma^2/(2\alpha)(1 - \exp -\alpha\tau)$. The first order perturbation of the stationary probability density function of the process A is:

$$P^{(1)}(A) = C \exp\left(-\frac{4}{\sigma^2} (V^{(0)}(A)) + \tilde{V}^{(1)}(A)\right) \tag{A.9}$$

which matches the expression in Eq. (29). The series expansion of the drift term perturbation $F^{(1)}(A, A_\tau)$ in Eq. (A.4) is needed only if one wishes to solve the integral in Eq. (A.6) exactly and recast a closed-form expression Eq. (29).

References

[1] M.R. Bothien, N. Noiray, B. Schuermans, A novel damping device for broadband attenuation of low-frequency combustion pulsations in gas turbines, *J. Eng. Gas Turbines Power* 136 (4) (2013) 041504, doi:10.1115/1.4025761.
 [2] G. Ghirardo, F. Boudy, M.R. Bothien, Amplitude statistics prediction in thermoacoustics, *J. Fluid Mech.* 844 (2018) 216–246, doi:10.1017/jfm.2018.173.
 [3] T. Lieuwen, Modeling premixed combustion-acoustic wave interactions: a review, *J. Propuls. Power* 19 (5) (2003) 765–781, doi:10.2514/2.6193.

- [4] N. Noiray, B. Schuermans, Deterministic quantities characterizing noise driven Hopf bifurcations in gas turbine combustors, *Int. J. Nonlinear Mech.* 50 (2013) 152–163, doi:[10.1016/j.ijnonlinmec.2012.11.008](https://doi.org/10.1016/j.ijnonlinmec.2012.11.008).
- [5] J. Rayleigh, *The explanation of certain acoustical phenomena*, *Nature* 18 (1878) 319–321.
- [6] P. Subramanian, R.I. Sujith, P. Wah, Subcritical bifurcation and bistability in thermoacoustic systems, *J. Fluid Mech.* 715 (2013) 210–238, doi:[10.1017/jfm.2012.514](https://doi.org/10.1017/jfm.2012.514).
- [7] J. Crawford, T. Lieuwen, Time delay and noise coupling in limiting control effectiveness in unstable combustors, 48th AIAA Aerospace Sciences Meeting Including the New Horizons Forum and Aerospace Exposition, American Institute of Aeronautics and Astronautics, Orlando, Florida, 2010, doi:[10.2514/6.2010-1519](https://doi.org/10.2514/6.2010-1519).
- [8] J.H. Crawford III, E.I. Verriest, T.C. Lieuwen, Exact statistics for linear time delayed oscillators subjected to Gaussian excitation, *J. Sound Vib.* 332 (22) (2013) 5929–5938, doi:[10.1016/j.jsv.2013.06.003](https://doi.org/10.1016/j.jsv.2013.06.003).
- [9] G. Ghirardo, M.P. Juniper, M.R. Bothien, The effect of the flame phase on thermoacoustic instabilities, *Combust. Flame* 187 (2018) 165–184, doi:[10.1016/j.combustflame.2017.09.007](https://doi.org/10.1016/j.combustflame.2017.09.007).
- [10] G. Bonciolini, A. Faure-Beaulieu, C. Bourquard, N. Noiray, Low order modelling of thermoacoustic instabilities and intermittency: flame response delay and nonlinearity, *Combust. Flame* 226 (2021) 396–411, doi:[10.1016/j.combustflame.2020.12.034](https://doi.org/10.1016/j.combustflame.2020.12.034).
- [11] N. Noiray, M. Bothien, B. Schuermans, Investigation of azimuthal staging concepts in annular gas turbines, *Combust. Theory Model.* 15 (5) (2011) 585–606, doi:[10.1080/13647830.2011.552636](https://doi.org/10.1080/13647830.2011.552636).
- [12] N. Noiray, B. Schuermans, On the dynamic nature of azimuthal thermoacoustic modes in annular gas turbine combustion chambers, *Proc. R. Soc. A* 469 (2151) (2013) 20120535, doi:[10.1098/rspa.2012.0535](https://doi.org/10.1098/rspa.2012.0535).
- [13] P. Clavin, J.S. Kim, F.A. Williams, Turbulence-induced noise effects on high-frequency combustion instabilities, *Combust. Sci. Technol.* 96 (1–3) (1994) 61–84, doi:[10.1080/00102209408935347](https://doi.org/10.1080/00102209408935347).
- [14] P.M. Morse, H. Feshbach, *Methods of Theoretical Physics, 1*, McGraw-Hill, New York, Toronto, London, 1953.
- [15] P.M. Morse, H. Feshbach, *Methods of Theoretical Physics, 2*, McGraw-Hill, New York, Toronto, London, 1953.
- [16] S. Candel, D. Durox, T. Schuller, J.-F. Bourgouin, J.P. Moeck, Dynamics of swirling flames, *Annu. Rev. Fluid Mech.* 46 (1) (2014) 147–173, doi:[10.1146/annurev-fluid-010313-141300](https://doi.org/10.1146/annurev-fluid-010313-141300).
- [17] A.P. Dowling, Y. Mahmoudi, Combustion noise, *Proc. Combust. Inst.* 35 (1) (2015) 65–100, doi:[10.1016/j.proci.2014.08.016](https://doi.org/10.1016/j.proci.2014.08.016).
- [18] F. Culick, L. Papparizos, J. Sterling, V. Burnley, Combustion noise and combustion instabilities in propulsion systems, *AGARD, Vol. 512*, Neuilly sur Seine, France, 1992.
- [19] G. Bonciolini, E. Boujo, N. Noiray, Output-only parameter identification of a colored-noise-driven Van-der-Pol oscillator: thermoacoustic instabilities as an example, *Phys. Rev. E* 95 (6) (2017) 062217, doi:[10.1103/PhysRevE.95.062217](https://doi.org/10.1103/PhysRevE.95.062217).
- [20] H. Chiu, M. Summerfield, Theory of combustion noise, *Acta Astronaut.* 1 (7–8) (1974) 967–984, doi:[10.1016/0094-5765\(74\)90063-0](https://doi.org/10.1016/0094-5765(74)90063-0).
- [21] G. Bonciolini, D. Ebi, E. Boujo, N. Noiray, Experiments and modelling of rate-dependent transition delay in a stochastic subcritical bifurcation, *R. Soc. Open Sci.* 5 (3) (2018) 172078, doi:[10.1098/rsos.172078](https://doi.org/10.1098/rsos.172078).
- [22] F. Culick, *Unsteady Motions in Combustion Chambers for Propulsion Systems*, Technical Report, NATO Research and Technology Organization, 2006.
- [23] V.S. Acharya, M.R. Bothien, T.C. Lieuwen, Non-linear dynamics of thermoacoustic eigen-mode interactions, *Combust. Flame* 194 (2018) 309–321, doi:[10.1016/j.combustflame.2018.04.021](https://doi.org/10.1016/j.combustflame.2018.04.021).
- [24] M. Lee, Y. Guan, V. Gupta, L.K.B. Li, Input-output system identification of a thermoacoustic oscillator near a Hopf bifurcation using only fixed-point data, *Phys. Rev. E* 101 (1) (2020) 013102, doi:[10.1103/PhysRevE.101.013102](https://doi.org/10.1103/PhysRevE.101.013102).
- [25] I.C. Waugh, M.P. Juniper, Triggering in a thermoacoustic system with stochastic noise, *Int. J. Spray Combust. Dyn.* 3 (3) (2011) 225–241, doi:[10.1260/1756-8277.3.3.225](https://doi.org/10.1260/1756-8277.3.3.225).
- [26] D. Mejia, M. Miguel-Brebion, L. Selle, On the experimental determination of growth and damping rates for combustion instabilities, *Combust. Flame* 169 (2016) 287–296, doi:[10.1016/j.combustflame.2016.05.004](https://doi.org/10.1016/j.combustflame.2016.05.004).
- [27] G. Ghirardo, M.P. Juniper, Azimuthal instabilities in annular combustors: standing and spinning modes, *Proc. R. Soc. A* 469 (2157) (2013) 20130232, doi:[10.1098/rspa.2013.0232](https://doi.org/10.1098/rspa.2013.0232).
- [28] A. Faure-Beaulieu, N. Noiray, Symmetry breaking of azimuthal waves: slow-flow dynamics on the Bloch sphere, *Phys. Rev. Fluids* 5 (2) (2020) 023201, doi:[10.1103/PhysRevFluids.5.023201](https://doi.org/10.1103/PhysRevFluids.5.023201).
- [29] T. Hummel, F. Berger, B. Schuermans, T. Sattelmayer, *Theory and modeling of non-degenerate transversal thermoacoustic limit cycle oscillations, Thermoacoustic Instabilities in Gas Turbines and Rocket Engines: Industry Meets Academia*, Munich, Germany, 2016.
- [30] T. Hummel, F. Berger, N. Stadlmair, B. Schuermans, T. Sattelmayer, Extraction of linear growth and damping rates of high-frequency thermoacoustic oscillations from time domain data, *J. Eng. Gas Turbines Power* 140 (5) (2018) 051505, doi:[10.1115/1.4038240](https://doi.org/10.1115/1.4038240).
- [31] X. Li, D. Zhao, X. Li, Effects of background noises on nonlinear dynamics of a modelled thermoacoustic combustor, *J. Acoust. Soc. Am.* 143 (1) (2018) 60–70, doi:[10.1121/1.5020059](https://doi.org/10.1121/1.5020059).
- [32] A.P. Dowling, S.R. Stow, Acoustic analysis of gas turbine combustors, *J. Propuls. Power* 19 (5) (2003) 751–764, doi:[10.2514/2.6192](https://doi.org/10.2514/2.6192).
- [33] M.R. Bothien, N. Noiray, B. Schuermans, Analysis of azimuthal thermo-acoustic modes in annular gas turbine combustion chambers, *J. Eng. Gas Turbines Power* 137 (6) (2015) 061505, doi:[10.1115/1.4028718](https://doi.org/10.1115/1.4028718).
- [34] N. Noiray, A. Denisov, A method to identify thermoacoustic growth rates in combustion chambers from dynamic pressure time series, *Proc. Combust. Inst.* 36 (3) (2017) 3843–3850, doi:[10.1016/j.proci.2016.06.092](https://doi.org/10.1016/j.proci.2016.06.092).
- [35] N. Noiray, Linear growth rate estimation from dynamics and statistics of acoustic signal envelope in turbulent combustors, *J. Eng. Gas Turbines Power* 139 (4) (2017) 041503, doi:[10.1115/1.4034601](https://doi.org/10.1115/1.4034601).
- [36] M.R. Bothien, J.P. Moeck, C.O. Paschereit, Comparison of linear stability analysis with experiments by actively tuning the acoustic boundary conditions of a premixed combustor, *J. Eng. Gas Turbines Power* 132 (12) (2010) 121502, doi:[10.1115/1.4000806](https://doi.org/10.1115/1.4000806).
- [37] E. Boujo, N. Noiray, Robust identification of harmonic oscillator parameters using the adjoint Fokker Planck equation, *Proc. R. Soc. A* 473 (2200) (2017) 20160894, doi:[10.1098/rspa.2016.0894](https://doi.org/10.1098/rspa.2016.0894).
- [38] C.F. Silva, W. Polifke, Non-dimensional groups for similarity analysis of thermoacoustic instabilities, *Proc. Combust. Inst.* 37 (4) (2019) 5289–5297, doi:[10.1016/j.proci.2018.06.144](https://doi.org/10.1016/j.proci.2018.06.144).
- [39] T. Insperger, G. Stépán, *Semi-Discretization for Time-Delay Systems: Stability and Engineering Applications*, Applied mathematical sciences, 178, Springer, New York, 2011.
- [40] N.K. Mukherjee, V. Shriya, Intrinsic flame instabilities in combustors: analytic description of a 1-D resonator model, *Combust. Flame* 185 (2017) 188–209, doi:[10.1016/j.combustflame.2017.07.012](https://doi.org/10.1016/j.combustflame.2017.07.012).
- [41] A. Orchini, C.F. Silva, G.A. Mensah, J.P. Moeck, Thermoacoustic modes of intrinsic and acoustic origin and their interplay with exceptional points, *Combust. Flame* 211 (2020) 83–95, doi:[10.1016/j.combustflame.2019.09.018](https://doi.org/10.1016/j.combustflame.2019.09.018).
- [42] E. Courtine, L. Selle, F. Nicoud, W. Polifke, C.F. Silva, M. Bauerheim, T. Poinso, *Causality and intrinsic thermoacoustic instability modes*, in: *Proceedings of the 2014 Summer Program - Center for Turbulence Research, Stanford (USA)*, 2014.
- [43] T.C. Lieuwen, Statistical characteristics of pressure oscillations in a premixed combustor, *J. Sound Vib.* 260 (1) (2003) 3–17, doi:[10.1016/S0022-460X\(02\)00895-7](https://doi.org/10.1016/S0022-460X(02)00895-7).
- [44] R. Stratonovich, *Topics in the Theory of Random Noise, 2*, Gordon Breach, New York, 1963.
- [45] J. Roberts, P. Spanos, Stochastic averaging: an approximate method of solving random vibration problems, *Int. J. Nonlinear Mech.* 21 (2) (1986) 111–134, doi:[10.1016/0020-7462\(86\)90025-9](https://doi.org/10.1016/0020-7462(86)90025-9).
- [46] P.-T.D. Spanos, Non-stationary random vibration of a linear structure, *Int. J. Solids Struct.* 14 (10) (1978) 861–867, doi:[10.1016/0020-7683\(78\)90076-8](https://doi.org/10.1016/0020-7683(78)90076-8).

- [47] J. Sanders, F. Verhulst, J. Murdock, *Averaging Methods in Nonlinear Dynamical Systems*, Applied Mathematical Sciences, 59, Springer New York, New York, NY, 2007, doi:[10.1007/978-0-387-48918-6](https://doi.org/10.1007/978-0-387-48918-6).
- [48] N.S. Krylov, N.N. Bogoliubov, *Introduction to Non-Linear Mechanics, II*, Princeton University Press, Princeton, 1947.
- [49] J.K. Hale, Averaging methods for differential equations with retarded arguments and a small parameter, *J. Differ. Equ.* 2 (1) (1966) 57–73, doi:[10.1016/0022-0396\(66\)90063-5](https://doi.org/10.1016/0022-0396(66)90063-5).
- [50] G. Medvedev, Asymptotic solutions of some systems of differential equations with deviating argument, *Sov. Math. Dokl.* 9 (1968) 85–87.
- [51] A. Halanay, On the method of averaging for differential equations with retarded argument, *J. Math. Anal. Appl.* 14 (1) (1966) 70–76, doi:[10.1016/0022-247X\(66\)90063-1](https://doi.org/10.1016/0022-247X(66)90063-1).
- [52] V. Foduck, The method of averaging for differential difference equations of the neutral type, *Ukr. Mat. Zhurnal* 20 (1968) 203–209.
- [53] C.W.S. To, *Nonlinear Random Vibration: Analytical Techniques and Applications*, CRC Press, 2017.
- [54] B. Lehman, V. Kolmanovskii, Extensions of classical averaging techniques to delay differential equations, in: *Proceedings of 1994 33rd IEEE Conference on Decision and Control*, Vol. 1, Lake Buena Vista, FL, USA, 1994, pp. 411–416, doi:[10.1109/CDC.1994.410893](https://doi.org/10.1109/CDC.1994.410893).
- [55] B. Lehman, S.P. Weibel, Fundamental theorems of averaging for functional differential equations, *J. Differ. Equ.* 152 (1) (1999) 160–190, doi:[10.1006/jdeq.1998.3523](https://doi.org/10.1006/jdeq.1998.3523).
- [56] M. Lakrib, On the averaging method for differential equations with delay, *Electron. J. Differ. Equ.* 2002 (65) (2002) 1–16.
- [57] M. Lakrib, T. Sari, Time averaging for ordinary differential equations and retarded functional differential equations, *Electron. J. Differ. Equ.* 2010 (40) (2010) 1–24.
- [58] Z.H. Wang, H.Y. Hu, A modified averaging scheme with application to the secondary Hopf bifurcation of a delayed van der Pol oscillator, *Acta Mech. Sin.* 24 (4) (2008) 449–454, doi:[10.1007/s10409-008-0170-1](https://doi.org/10.1007/s10409-008-0170-1).
- [59] S. Wirkus, R. Rand, The dynamics of two coupled van der Pol oscillators with delay coupling, *Nonlinear Dyn.* 30 (3) (2002) 205–221, doi:[10.1023/A:1020536525009](https://doi.org/10.1023/A:1020536525009).
- [60] M. Gluzman, R. Rand, Dynamics of Two Coupled van der Pol Oscillators with Delay Coupling Revisited, arXiv:[1705.03100](https://arxiv.org/abs/1705.03100)(2017).
- [61] S.M. Sah, R.H. Rand, Delay Terms in the Slow Flow, arXiv:[1601.01853](https://arxiv.org/abs/1601.01853)(2016).
- [62] V.B. Kolmanovskii, Stability of functional differential equations, in: *North-Holland Series in Applied Mathematics and Mechanics*, 38, Elsevier, 1994, pp. 501–549, doi:[10.1016/B978-0-444-81951-2.50012-5](https://doi.org/10.1016/B978-0-444-81951-2.50012-5).
- [63] A. Orchini, S. Illingworth, M. Juniper, Frequency domain and time domain analysis of thermoacoustic oscillations with wave-based acoustics, *J. Fluid Mech.* 775 (2015) 387–414, doi:[10.1017/jfm.2015.139](https://doi.org/10.1017/jfm.2015.139).
- [64] L. Kabiraj, R.I. Sujith, Nonlinear self-excited thermoacoustic oscillations: intermittency and flame blowout, *J. Fluid Mech.* 713 (2012) 376–397, doi:[10.1017/jfm.2012.463](https://doi.org/10.1017/jfm.2012.463).
- [65] U. Küchler, E. Platen, Strong discrete time approximation of stochastic differential equations with time delay, *Math. Comput. Simul.* 54 (1–3) (2000) 189–205, doi:[10.1016/S0378-4754\(00\)00224-X](https://doi.org/10.1016/S0378-4754(00)00224-X).
- [66] U. Küchler, E. Platen, Weak discrete time approximation of stochastic differential equations with time delay, *Math. Comput. Simul.* 59 (6) (2002) 497–507, doi:[10.1016/S0378-4754\(01\)00431-1](https://doi.org/10.1016/S0378-4754(01)00431-1).
- [67] B. Picinbono, On instantaneous amplitude and phase of signals, *IEEE Trans. Signal Process.* 45 (3) (1997) 552–560, doi:[10.1109/78.558469](https://doi.org/10.1109/78.558469).
- [68] P.D. Spanos, I.A. Kougioumtzoglou, K.R.M. dos Santos, A.T. Beck, Stochastic averaging of nonlinear oscillators: hilbert transform perspective, *J. Eng. Mech.* 144 (2) (2018) 04017173, doi:[10.1061/\(ASCE\)EM.1943-7889.0001410](https://doi.org/10.1061/(ASCE)EM.1943-7889.0001410).
- [69] T.D. Frank, Delay Fokker–Planck equations, perturbation theory, and data analysis for nonlinear stochastic systems with time delays, *Phys. Rev. E* 71 (3) (2005) 031106, doi:[10.1103/PhysRevE.71.031106](https://doi.org/10.1103/PhysRevE.71.031106).
- [70] T.D. Frank, P.J. Beek, R. Friedrich, Fokker–Planck perspective on stochastic delay systems: exact solutions and data analysis of biological systems, *Phys. Rev. E* 68 (2) (2003) 021912, doi:[10.1103/PhysRevE.68.021912](https://doi.org/10.1103/PhysRevE.68.021912).
- [71] T. Frank, Stochastic systems with delay: perturbation theory for second order statistics, *Phys. Lett. A* 380 (14–15) (2016) 1341–1351, doi:[10.1016/j.physleta.2016.02.011](https://doi.org/10.1016/j.physleta.2016.02.011).
- [72] S. Guillouic, I. L’Heureux, A. Longtin, Small delay approximation of stochastic delay differential equations, *Phys. Rev. E* 59 (4) (1999) 3970–3982, doi:[10.1103/PhysRevE.59.3970](https://doi.org/10.1103/PhysRevE.59.3970).